

國立交通大學
光電工程研究所
碩士論文

利用時間解析量測技術研究氮砷化銦鎵量子井的超快
載子動力行為



Ultrafast Carrier Dynamics of $\text{InGaAs}_x\text{N}_{1-x}$ Single
Quantum Wells by Time-Resolved Photoreflectance
Measurement

研究生：陳穎書

指導教授：謝文峰教授

中華民國九十六年六月

利用時間解析量測技術研究氮砷化銦鎵 量子井的超快載子動力行為

Ultrafast Carrier Dynamics of InGaAs_xN_{1-x} Single Quantum
Wells by Time-Resolved Photoreflectance Measurement

研究生：陳穎書

Student: Ying-Shu Chen

指導教授：謝文峰 教授

Advisor: Dr. Wen-Feng Hsieh



A Thesis

Submitted to Institute of Electro-Optical Engineering

College of Electrical and Computer Engineering

National Chiao Tung University

in Partial Fulfillment of the Requirements

for the Degree of

Master

in

Electro-optical Engineering

June 2007

Hsin-chu, Taiwan, Republic of China

中華民國九十六年六月


利用時間解析量測技術研究氮砷化銦鎵 量子井的超快載子動力行為

研究生：陳穎書

指導教授：謝文峰教授

國立交通大學光電工程研究所

摘要



在本論文中，我們比較由金屬有機化學氣相沈積法(MOCVD)成長的砷化銦鎵和氮砷化銦鎵單層量子井的超快載子動力學。氮砷化銦鎵的能隙因為氮的加入比砷化銦鎵的能隙小很多，可以發出波長為 $1.45 \mu\text{m}$ 的光。我們利用飛秒時析反射量測研究載子的鬆弛過程。比較這兩個樣品在不同波長的量測結果，發現短波長下由於能隙收縮，反射率變化為負；長波長下由於能帶填充，反射率變化則為正。另外(氮)砷化銦鎵有兩個生命期，我們推測較短者為電子電洞散射所致，較長者在砷化銦鎵和氮砷化銦鎵中，分別為熱聲子效應和受激輻射。

Ultrafast Carrier Dynamics of InGaAs_xN_{1-x} Single Quantum Wells by Time Resolved Photoreflectance Measurement

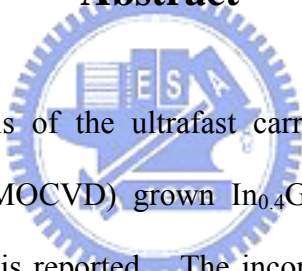
Student: Ying-Shu Chen

Advisor: Dr. Wen-Feng Hsieh

Institute of Electro-Optical Engineering

National Chiao Tung University

Abstract



The comparative analysis of the ultrafast carrier dynamics of metal-organic chemical vapor deposition (MOCVD) grown In_{0.4}Ga_{0.6}As and In_{0.4}Ga_{0.6}As_{0.98}N_{0.02} single quantum wells (SQW) is reported. The incorporation of a low content N in InGaAsN reduces the band-gap energy significantly and allows emission wavelengths shift to 1.45 μm. Carrier dynamics were investigated by femtosecond time-resolved photoreflectance measurement at 800/820 and 880 nm with various pump intensities. Comparison with these two samples at different pumping wavelengths indicates that ΔR is negative at pumping wavelength < 820nm due to bandgap renormalization; ΔR is positive at 880nm due to band filling effect. Furthermore, there are two lifetimes in InGaAs(N), and we speculate that the shorter one is due to electron-hole scattering. The longer one is due to hot phonon decay in InGaAs and stimulated emission in InGaAsN.

致謝

我在這兒為青春畫了一個小小的句點。我大哭、也大笑過，那些曾有過的燦爛和心碎都在本論文完成的當下化為雲煙，但永遠不會被忘記。

兩年來最要感謝的是謝老師文峰，因為您的悉心指導和對學生的用心，讓我順利地完成了學位。謝謝家弘學長指引的方向；謝謝智章學長總是耐心解答我的疑問，陪伴我度過一個又一個的難關；謝謝佩兒學妹在物理年會的前後與我同甘共苦；謝謝小波波不厭其煩地教我實驗的技巧，聽我抱怨，給我安慰。也謝謝實驗室眾多的博班學長姐們，黃董、晴如、至賢、維仁、國峰、民哥，為了實驗室不停地努力著。

常常與我分享心事的松哥，你讓我覺得好受重視；小豪和 IC，因為有你們，我們有好多漂亮的照片；Bogi，我喜歡和善良的你聊天，那是種享受；李兩光，以後變成股票大亨不要忘記學姐啊；賴小妹，妳真的是個無法用筆墨形容的有趣孩子；文藝青年林先生易慶，畢業典禮的花很令人感動呢；徐瑋澤和陳厚仁，都是認真的好學弟。

碩二的夥伴們，你們個個都特色十足。變態偷拍色老頭 Leader 阿徐，雖然你偽裝了近一年半的自己，但最後半年的狐狸尾巴還是露出來了吧，非常遺憾沒有大顯身手在你的臉上留下我藝術的痕跡。超變態兇猛又三八的娘飛飛，不停地挑戰我的極限，讓我的耐力指數急速飆升。超超變態暴力又阿呆的郭憨憨，我不懂你為何不了解我真的比你聰明，很多。我深深地感謝你們，帶給了我無數的歡笑。阿徐，謝謝你在我難過的時候摸著我的頭給了一句加油；義氣郭，你半夜三點洗 sample 的行為，沒齒難忘；娘飛飛，你是天上掉下來的禮物，讓我更堅強。

偶爾很可口的冬山河，認識你很開心，你是個身手敏捷、溫柔且耐性十足的好男生。魅力獅子王阿丹，「干你屁事」真的非常好用，謝謝妳接送了我們這許多的日子，陪我們打球，妳是個很好的朋友喔；蔡明阿屁，我一點不在意妳總是誤會自己 elegant，因為我們一同走過了這麼多風風雨雨，一輩子都會互相扶持的；無助時候妳放在肩上的手，傾聽時候妳專注的眼神，故意嘲笑的鼻孔哼氣聲，我都會牢牢記住。當初一起找到這間實驗室，很棒吧。

特別感謝活了三千年的龍先生，幫我掃了一年的廁所、洗了好多次衣服，跟你當室友真好！親愛的爸爸媽媽，可愛的弟弟，謝謝你們讓我知道不管發生了什麼事，身後總會有個在等待我的家。永遠帶著微笑和諒解的廷廷，謝謝你付出了無數的包容和扶持，實驗做不出來時候任性著想放棄的念頭，都因為你給的安心

而消散了。如果我有一點點的勇敢或樂觀，你絕對功不可沒。

還有眾多好友的陪伴和鼓勵，無法逐一感謝。那杯溫熱的牛奶、那個粉紅色的五角大星星、那句 msn 上的加油暱稱，我全都收到心裡了，身邊擁有的真的太多、太多。

踏出這個校門之後，就要成為成熟的大人了。久遠的未來來不及想到，但我會懷抱著現在的美好，一步一步往下走去。

最後感謝國科會計畫 NSC-95-2221-E-009-308 對此研究的支持和贊助。

穎書于交大
2007.7.17



Content

Abstract (in Chinese).....	I
Abstract (in English).....	II
Acknowledgements.....	III
Contents.....	V
List of Tables.....	VII
List of Figures.....	VIII
Chapter 1 Introduction.....	1
1-1 InGaAs(N)/GaAs Heterostructures.....	1
1-2 Ultrafast Carrier Dynamics in Semiconductors.....	2
1-3 Femtosecond Pump-Probe Technique.....	5
1-4 Aim of this thesis.....	7
Chapter 2 Ultrafast Spectroscopy of Semiconductors	9
2-1 Background Concepts.....	9
2-1.1 Carrier Relaxation Regimes.....	9
2-1.2 Scattering Processes in Semiconductors.....	12
2-2 Carrier-Induced Change in Refractive Index.....	13
2-2.1 Band Filling.....	13
2-2.2 Bandgap Renormalization.....	15
2-2.3 Free Carrier Absorption.....	16

Chapter 3	Experiments.....	18
3-1	Principle of Femtosecond Time-Resolved Measurement.....	18
3-2	Experimental System of Femtosecond Time-Resolved Measurement.....	21
3-2.1	Ultrafast Laser System.....	21
3-2.2	Autocorrelator.....	22
3-2.3	Experimental Setup of Pump-probe Measurement.....	24
3-3	Zero Delay Point of the System.....	25
3-4	InGaAsN Single Quantum Well Structures.....	26
3-5	Method and Steps of Pump-probe Measurement.....	27
Chapter 4	Results and Discussion.....	29
4-1	Ultrafast Time-Resolved Photoreflectance of $\text{In}_{0.4}\text{Ga}_{0.6}\text{As}_{1-x}\text{N}_x$ SQW.....	31
4-2	Carrier Relaxation Time of $\text{InGaAs}_{1-x}\text{N}_x$ SQW.....	40
Chapter 5	Conclusion and Perspectives.....	45
	References.....	46

List of Figures

Fig. 1-1	The electron-hole pair creation following excitation.....	4
Fig. 1-2	The energy in a photoexcited semiconductor.....	4
Fig. 1-3	Different time-scale measurements require different tools...	6
Fig. 1-4	The shortest pulses versus years.....	7
Fig. 2-1	Four temporally overlapping relaxation regimes.....	11
Fig. 2-2	Bandfilling nonlinearity in a narrow-gap semiconductor...	14
Fig. 3-1	The principle of pump-probe technique.....	20
Fig. 3-2	The optical beam path within Coherent Mira-900.....	21
Fig. 3-3	Sketch diagram of the intensity autocorrelator.....	23
Fig. 3-4	The autocorrelator trace.....	23
Fig. 3-5	Femtosecond time-resolved photoreflectance measurement system.....	25
Fig. 3-6	Band diagram of the $\text{In}_{0.4}\text{Ga}_{0.6}\text{As}_{1-x}\text{N}_x$ SQW.....	27
Fig. 3-7	HRTEM image of $\text{In}_{0.4}\text{Ga}_{0.6}\text{As}_{0.995}\text{N}_{0.005}/\text{GaAs}$ SQW.....	27
Fig. 4-1	Absorption curve of GaAs.....	30
Fig. 4-2	The pump-intensity dependent time-resolved photoreflectance of $\text{In}_{0.4}\text{Ga}_{0.6}\text{As}_{1-x}\text{N}_x$ SQW pumped at 800/820 nm.....	33
Fig. 4-3	The pump-intensity dependent time-resolved photoreflectance of $\text{In}_{0.4}\text{Ga}_{0.6}\text{As}_{1-x}\text{N}_x$ SQW pumped at 880 nm.....	35
Fig. 4-4	The measured ΔR peak amplitude versus pumping power	39
Fig. 4-5	The carrier lifetime versus pumping power in $\text{In}_{0.4}\text{Ga}_{0.6}\text{As}$ SQW.....	41
Fig. 4-6	The carrier lifetime versus pumping power in $\text{In}_{0.4}\text{Ga}_{0.6}\text{As}_{0.995}\text{N}_{0.002}$ SQW.....	43

List of Tables

Table 1-1	Fundamental processes in semiconductors.....	5
Table 4-1	List of carrier dynamics of $\text{In}_{0.4}\text{Ga}_{0.6}\text{As}_{1-x}\text{N}_x$ SQW with various pumping power.....	37



Chapter 1 Introduction

1-1 InGaAs(N)/GaAs Heterostructures

Dilute quaternary solid solution of $\text{In}_y\text{Ga}_{1-y}\text{As}_{1-x}\text{N}_x$ ($x < 0.1$) is of much interest to various electronic and optoelectronic applications due to the highly nonlinear effects upon nitrogen incorporation. This characteristic can be used to fabricate laser diodes for 1.2-1.3 μm spectral range on cheap GaAs substrates instead of expensive InP substrates which is for InGaAsP/InP system [1]. The large band offsets are due to the large electronegativity of N atoms that pulls down both conduction and valence band edges in InGaAsN quaternary alloy and leads to better electron confinement. Finally the temperature performance will be better than the conventional InP-based materials [2][3]. High-performance InGaAs(N) single quantum well (SQW) lasers which raise lasing emission wavelength extended to 1300 nm at room temperature have been realized by Tansu *et al.* lately [4][5][6]. They also have the potential to be long wavelength photonic communication devices [7].

Some experimental results of the fundamental properties of InGaAsN semiconductor have been reported. They have shown the potential applications of InGaAs(N) in the telecommunication field. Time-resolved measurements of carrier dynamics in bulk and quantum-well InGaAs using differential absorption spectroscopy was presented by Sucha *et al.* [8] in 1994. They found that for sample from 100 to 6000Å, the carrier thermalization time is 200-300 fs regardless of the layer width. Borri *et al.* [9] used the time-integrated four-wave mixing method to study the temperature and density dependences of exciton dephasing time in $\text{In}_{0.18}\text{Ga}_{0.82}\text{As}/\text{GaAs}$ single quantum well. Bhattacharya *et al.* [10] performed pump-probe differential transmission in $\text{In}_{0.4}\text{Ga}_{0.6}\text{As}/\text{GaAs}/\text{AlGaAs}$ heterostructures.

D. E. Mars *et al.* [11] have grown InGaAsN quantum well laser by MBE and done the room temperature photoluminescence (PL) measurements. J. Misiewicz *et al.* investigated the influence of nitrogen on carrier localization in InGaAsN/GaAs single quantum well with nitrogen concentration up to 5.2%. A. Vinattieri *et al.* [12] discovered the exciton dynamics in InGaAsN/GaAs quantum well structures after picosecond excitation. They also did the PL measurements for different nitrogen content situations. LiFang Xu *et al.* [13] quantitatively analyzed the relative contribution of free excitons and free carriers to the radiative recombination at different temperature.

O. Anton *et al.* [4] reported the behavior of the carrier lifetime with carrier density on two different nitrogen contents in InGaAs_{1-x}N_x single quantum well laser diodes. When nitrogen is added into the well, the recombination lifetime is significantly reduced. These samples were also found that behave like a quantum-dot and affect the carrier dynamics by localization for temperature from 15 to 150K in CLEO 2005 [14]. The material properties of III-V-N compounds have been accounted interesting behaviors and been studied vitally during recent years.

1-2 Ultrafast Carrier Dynamics in Semiconductors

The carrier relaxation processes in the semiconductor laser which had been widely investigated strongly affect the characteristics and performance of it [15]-[19]. Over the past few decades, there have been huge advancements in the field of ultrafast carrier dynamics in bulk and quantum confined semiconductors [20]. There are two driving forces behind the development: one is the importance in solid-state physics that the ultrafast optical technique opened up the subpicosecond and femtosecond time domains, and the other is the infinite need for fast response of high-speed

microelectronic devices. Basic understanding of the various carrier dynamical processes in semiconductors helps people to realize the principle of manufacturing those devices.

The excitation of semiconductors through equilibrium and the subsequent relaxation processes with different rates has become important in semiconductor field. Fig. 1-1 shows that when the photon energy is larger than the fundamental energy gap, linear absorption occurs. After the optical or electrical excitation of carriers, there are various microscopic processes of momentum and energy relaxation of carriers in the semiconductor such as carrier-carrier scattering, optical phonon scattering, intervalley scattering, etc., that occur in the femtosecond to picosecond time scale. These processes are listed in Table 1-1 and the energy relaxation after excitation is shown in Fig. 1-2. In order to investigate such a short interaction time, femtosecond pump-probe measurements, including differential transmission, reflection, and absorption spectroscopies using ultrashort pulse lasers as the exciting sources, have been widely used for III-V semiconductors [21][22].

In this thesis, we have investigated the processes such as carrier thermalization, bandgap renormalization, and energy relaxation on bulk GaAs-based materials at room temperature. There will be many benefits to realize the relaxation mechanisms of carriers in materials for manufacturing high-speed photonic devices. Furthermore, bulk GaAs-based materials which emit fluorescence at 1.2-1.5 μm have a lot of potential in long wavelength band.

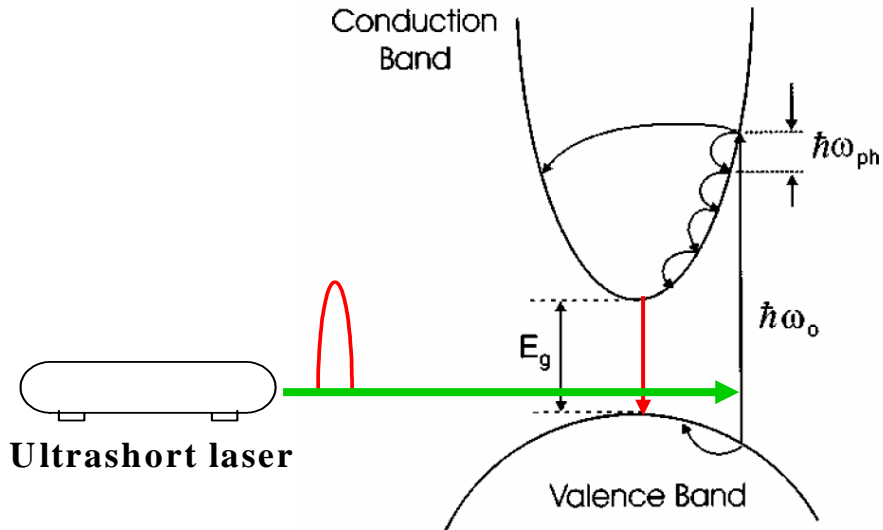


Fig. 1-1 The electron-hole pair creation following excitation of a semiconductor with laser radiation of energy $\hbar\omega_0$.

Energy relaxation follows via optical phonon emission ($\hbar\omega_{ph}$).

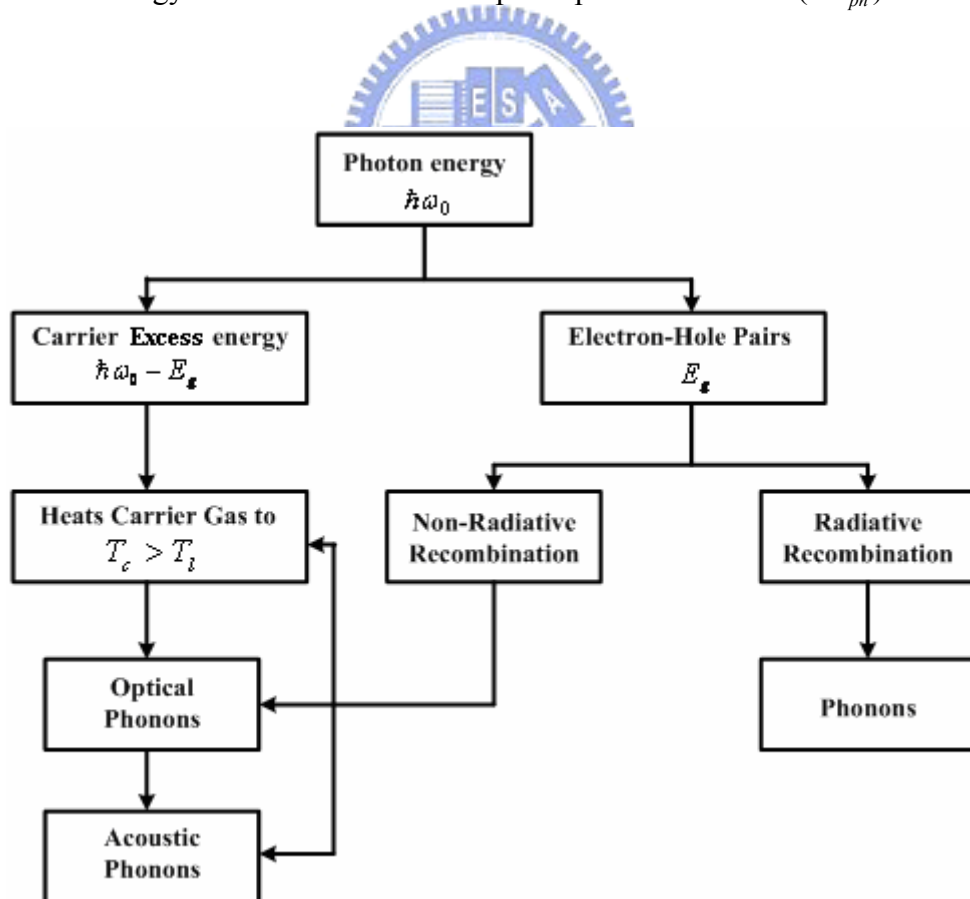


Fig. 1-2 The block diagram illustrating the follow of energy in a photoexcited semiconductor.

Table 1-1 Fundamental processes in semiconductors.

Microscopic process	Characteristic time (s)
Carrier-carrier scattering	$10^{-15}\sim 10^{-12}$
Intervalley scattering	$>10^{-14}$
Intravalley scattering	$\sim 10^{-13}$
Carrier-optical phonon thermalization	$>10^{-12}$
Optical phonon-acoustic phonon interaction	$\sim 10^{-11}$
Carrier diffusion (0.1 μm)	$\sim 10^{-11}$
Auger recombination (carrier density 10^{20} cm^{-3})	$\sim 10^{-10}$
Radiative recombination	$>10^{-9}$
Lattice heat diffusion (1 μm)	$\sim 10^{-8}$

1-3 Femtosecond Pump-Probe Technique

Imagine if we want to measure the speed of a running turtle, we only need a minute-resolution clock. But for measuring the speed of a running man, a second-resolution stopwatch may be required. Different time-scale measurements require different time-resolution tools as shown in Figure 1-3. The femtosecond-resolution pump-probe technique with ultrashort pulse laser can achieve the goal of measuring electron lifetime between various energy bands. In this technique, a femtosecond laser pulse is separated into two beams, a pump and a probe beam, with optical time delay between them. The pump beam should cover the probe beam completely and they overlap spatially on the sample under investigation. After pump beam exciting the samples, there will be a change of absorption coefficient on them. The probe beam is for detecting these changes. The time evolution of the excited states is prospected by varying the time delay. Although we adjust the phase of pump and probe beams perpendicular to each other, coherent artifact which is due to an additional coupling between the two beams is still unavoidable over the region near zero time delay where they interact coherently.

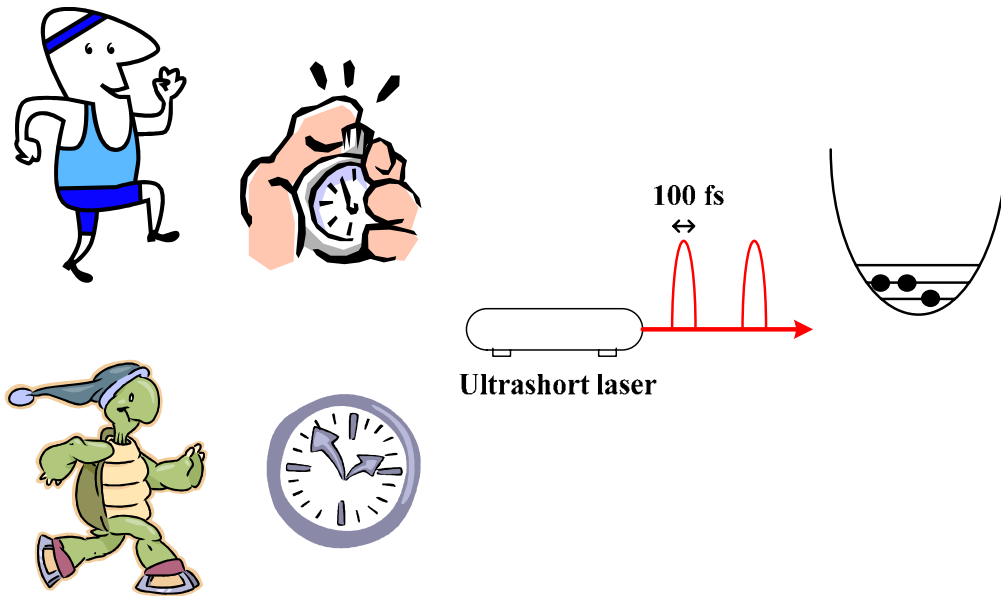


Fig. 1-3 Illustrating different time-scale measurements require different time-resolution tools.

Fig. 1-4 exhibits the technology of generating and detecting short pulses in the pasts few decades. The width of optical pulses has fallen by more than three orders of magnitude since 1966. Fork and Shank developed the colliding pulse mode-locked (CPM) laser in 1981 [23], which made the femtosecond resolution measurement of semiconductors possible.

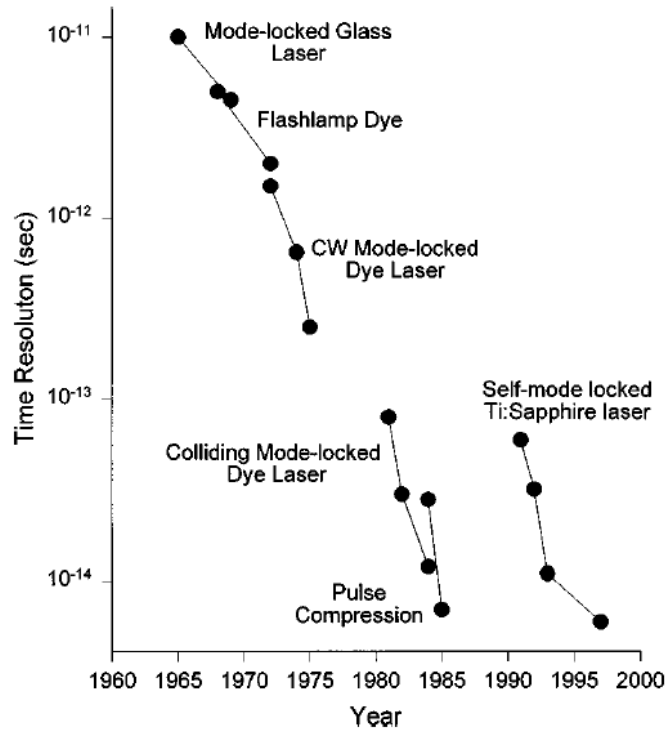
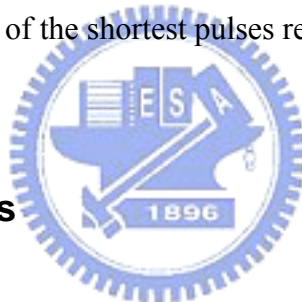


Fig. 1-4 Schematic diagram of the shortest pulses reported versus years. (Ref. 12)



1-4 Aim of this thesis

In this thesis, we study the ultrafast time-resolved photoreflectance of $\text{In}_{0.4}\text{Ga}_{0.6}\text{As}_{1-x}\text{N}_x/\text{GaAs}$ single quantum wells. We compare the pump-probe measurements in samples differing in the nitrogen incorporation ($x = 0\%$ and 2%) and in the laser wavelengths ($\lambda = 820 \text{ nm}$ and $\lambda = 880 \text{ nm}$). At $\lambda = 880 \text{ nm}$, it can prevent the absorption of confining layer GaAs whose bandgap is about 870 nm .

Chapter 2 presents the background concepts and theorems of the ultrafast spectroscopy of semiconductors. Section 2-1 introduces the scattering processes and carrier relaxation regimes in semiconductors. Then we focus on the reasons of changing in refractive index which includes band filling effect, bandgap renormalization and free carrier absorption.

Chapter 3 describes the sample structure and experimental setup of ultrafast

time-resolved measurement. Chapter 4 shows the results and analysis of our measurements. We have discovered large different phenomena with pumping wavelength at 820 and 880 nm. The change of reflection is negative and positive, respectively. Finally, the perspectives are discussed in Chapter 5.



Chapter 2 Ultrafast Spectroscopy of Semiconductors

2-1 Background Concepts

2-1.1 *Carrier Relaxation Regimes*

After an ultrashort pulse is sent into a semiconductor, it will be excited to higher energy level and then undergoes several stages of relaxation before it returns back to thermodynamic equilibrium [24]. There are four temporally overlapping regimes of the carrier relaxation:

(a) **Coherent Regime**

When a semiconductor is excited by an ultrashort pulse, the excitation in the semiconductor will have well-defined phase relationship within itself and with the electromagnetic field which created the excitations. The excitation can be either real or virtual. The scattering processes in semiconductors that destroy the coherence are exceedingly fast that requires pico- and femtosecond techniques to study. Coherent regime exhibits a lot of fascinating phenomena with basic quantum mechanics in semiconductors.

(b) **Non-thermal Regime**

In this regime, the excitation is real. After dephasing free electron-hole pairs and excitons in the coherent regime, the distribution of excitation (i.e. free electron-hole pairs or excitons) is likely to be non-thermal. It means the distribution function can not be represented by a temperature. This regime includes various processes such as carrier-carrier scattering or exciton-exciton scattering. Through the scatterings

above, it takes the non-thermal distribution to a hot, thermalized distribution.

(c) Hot-Carrier Regime

Energy redistribution within the carrier or exciton system is due to carrier-carrier or exciton-exciton scattering. The procedure leads to a thermalized distribution function of carriers or excitons which can be expressed by a temperature. The temperature is often higher than the lattice temperature, and might be different for various sub-systems. The times of thermalization depend on many factors, for example, carrier density. The electrons and holes thermalize among themselves in hundreds of femtoseconds, while they achieve an ordinary temperature in a few picoseconds. Those thermalized electron-hole pairs take hundreds of picoseconds to reach lattice temperatures, and this process is under interaction with several kinds of phonons in the semiconductor.

Investigation of this regime concentrates on the rate of cooling of carriers to the lattice temperature and the various scattering processes.

(d) Isothermal Regime

All the carriers, phonons, and excitons relax to equilibrium with one another at the end of hot-carrier regime. Yet there are still some electrons and holes exceeding the thermodynamic equilibrium. In isothermal regime, these excess electron-hole pairs or excitons recombine one another radiatively or non-radiatively then return the semiconductor to the thermodynamic equilibrium.

The schematic diagram of these four regimes is illustrated in Figure 2-1. The figure shows some typical processes occurring in each relaxation regimes. The time scale for each event relies vigorously on band structure, excess energy, the nature of

the excitation, the density of excitation, and the lattice temperature...etc.

We should emphasize that many of the physical relaxation in the different regimes are occurring simultaneously and the four relaxation regimes is used for convenience to describe the dynamics of carrier relaxation. For instance, the processes that destroy coherence perhaps also contribute to thermalization of carrier distribution functions, and emission of phonons may take place while the electrons and holes are thermalizing to a hot distribution. The non-thermal carrier distribution function created by an ultrashort pulse is affected by the dephasing of coherent polarization during the pulse. Figure 2-1 is the relaxation regimes under different time scales.

Coherent Regime ($\leq 200\text{fs}$)

- ◆ Momentum scattering
- ◆ Carrier-carrier scattering
- ◆ Intervally scattering ($\Gamma \rightarrow L, X$)
- ◆ Hole-optical-phonon scattering

Non-thermal Regime ($\leq 2\text{ps}$)

- ◆ Electron-hole scattering
- ◆ Electron-optical-phonon scattering
- ◆ Intervally scattering ($L, X \rightarrow \Gamma$)
- ◆ Carrier capture in quantum wells
- ◆ Intersubband scattering ($\Delta E > \hbar \omega_{LO}$)

Hot-excitation Regime ($\sim 1-100\text{ps}$)

- ◆ Hot-carrier-phonon interactions
- ◆ Decay of optical phonons
- ◆ Carrier-acoustic-phonon scattering
- ◆ Intersubband scattering ($\Delta E < \hbar \omega_{LO}$)

Isothermal Regime ($\geq 100\text{ps}$)

- ◆ Carrier recombination

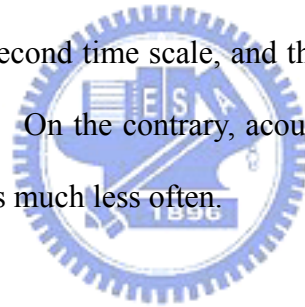
Fig. 2-1 Four temporally overlapping relaxation regimes in photoexcited semiconductors.

2-1.2 Scattering Processes in Semiconductors

There are various kinds of scattering mechanisms. The interactions of electrons, holes, excitons, and phonons will result in different relaxation times in a semiconductor. We will briefly discuss several scattering mechanisms in the following subsections [24].

(a) Carrier-Phonon Interactions

Interaction among carriers and phonons plays an important role in the exchange of energy and momentum between the lattice and carriers, and then determines the relaxation procedure of photoexcited semiconductors. Optical phonon and intervally scatterings proceed in a picosecond time scale, and they are the most frequent events in carrier-phonon interaction. On the contrary, acoustic phonon scattering occurs in a nanosecond time scale and is much less often.



(b) Carrier-Carrier Scattering

Carrier-carrier scattering is accountable for the thermalization of photoexcited non-thermal carriers. The process is judged by Coulomb interaction. It mainly determines the exchange of energy between carriers, and it contains electron-electron, hole-hole, and electron-hole scattering.

(c) Hot Phonons

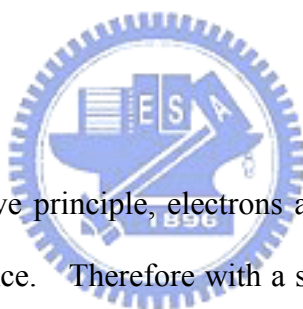
When a laser beam is incident into a material, the density of photoexcitation will be moderate to high, and a lot of phonons may be generated as the carriers relax by the emission of phonons. The optical phonons near the zone center have a low dispersion so that their group velocities are small and the generated phonons are

unlikely to leave the photoexcited volume. In this case, the decay time is found to be several picoseconds that a large non-equilibrium phonon population (hot phonons) is created at moderate to high photoexcitation density.

Other scattering processes specific to quantum wells are also significant, such as inter-subband scattering, capture of carriers from the barriers into wells, and real space transfer of carriers from quantum wells into the barriers. These are not the primary processes in our experiments, so we will not put emphasis on them in this article

2-2 Carrier-Induced Change in Refractive Index

2-2.1 Band Filling



According to Pauli exclusive principle, electrons and holes as Fermions can only occupy each quantum state once. Therefore with a spin-up and a spin-down carrier, each \mathbf{k} state in a semiconductor band can be occupied twice. The carriers in quasi-equilibrium occupy the energetically lowest state first due to the principle of energy minimization. Finally, the states in the bottom of the conduction band will be filled with electrons and in the top of the valence band will be filled with holes. When pumping energy is above the bandgap, carriers will be excited toward higher states and the absorption coefficient α will decrease. Figure 2-2 is a schematic of the bandfilling process [25].

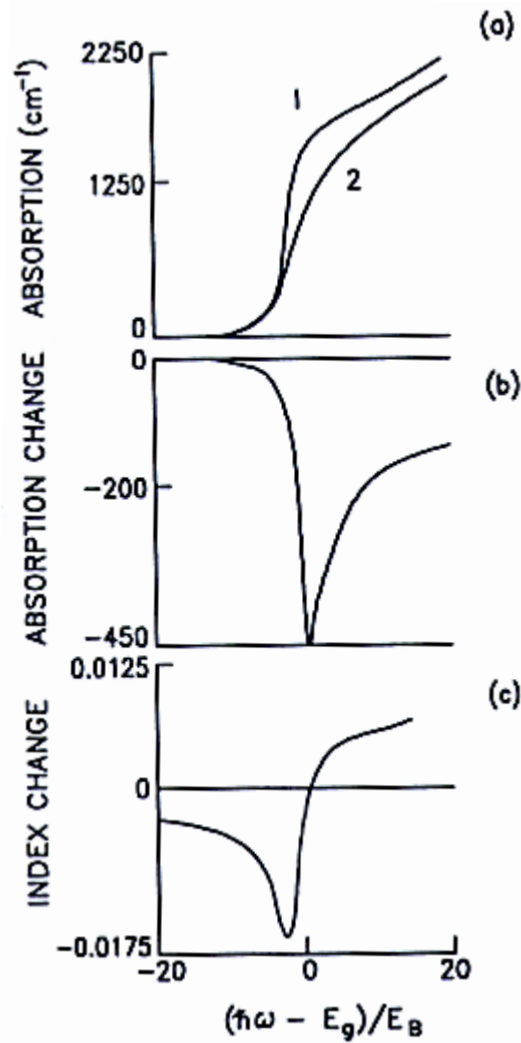


Fig. 2-2 Bandfilling nonlinearity in a narrow-gap semiconductor.

- (a) The absorption spectra at low temperatures for low (curve 1) and high (curve 2) carrier densities. (b) The change in the absorption coefficient, $\Delta\alpha$. (c) The change in the refractive index, $\Delta n(\omega)$.

The Fermi functions for the electrons (f_e) and holes (f_h) can only vary between 0 and 1. If we denote energy in the valence band by E_v and in the conduction band by E_c , then the absorption coefficient of an injected semiconductor is

$$\alpha(N, P, E) = \alpha_0(E) [f_v(E_v) - f_c(E_c)],$$

where α_0 is the density of states near the bandgap in a pure direct-gap semiconductor with

no injection which is given by the square-root law: $\alpha_o(E) = \frac{C}{E} \sqrt{E - E_g}$, $E \geq E_g$, f_v is the probability of an electron occupying a valence band state, and f_c is the probability of a hole occupying a conduction band state. N and P are the concentrations of free electrons and holes, respectively. Band filling results in a change of the absorption coefficient $\Delta\alpha(N, P, E) = \alpha_o(E)[f_v(E_v) - f_c(E_c) - 1]$. Near the conduction and valence band edges, we know that $f_c > 0$ and $f_v < 1$ with carrier injection. This equation leads to a negative change of absorption coefficient, which means the band filling effect decreases α at a fixed incident photon energy.

The real and imaginary parts of the refractive index $n-i\kappa$ are related to each other by Kramers-Kronig (KK) integrals: $n(E) = 1 + \frac{2c\hbar}{e^2} \text{P} \int_0^\infty \frac{\alpha(E')}{E'^2 - E^2} dE'$, where c is the

speed of light, e is the electron charge, $\alpha = \frac{4\pi\kappa}{\lambda}$, E is the photon energy, and P stands for the principle value of the integral. We define the change of refractive index as $\Delta n(N, P, E) = n(N, P, E) - n_o(E)$, where n_o is the refractive index in the material with no injection. We can get the change of refractive index from the

formula above: $\Delta n(N, P, E) = \frac{2c\hbar}{e^2} \text{P} \int_0^\infty \frac{\Delta\alpha(N, P, E')}{E'^2 - E^2} dE'$. Carrier injection results in

$\Delta\alpha$, and $\Delta\alpha$ leads to Δn . After calculation, the refractive index increases at energies above E_g and vice versa.

2-2.2 Bandgap Renormalization

Fermions with parallel spin can not sit in the same unit cell. Since this situation would occur for a random distribution, but does not for fermions, we can conclude that the exchange energy increases the average distance between electrons with

parallel spin and consequently reduces their total repulsive Coulomb energy. The reduction of a repulsive energy term means a lowering of the total energy of the electron system.

The correlation energy describes that the electron-hole pair system can lower its energy, if the distribution of electrons and holes relative to each other is not random. The change of Coulomb force leads to a change of atom's potential, and then a change of band gap.

Wolff first derived the expression for the band gap renormalization: $\Delta E_g = -\left(\frac{e}{2\pi\epsilon_o\epsilon_s}\right)\left(\frac{3n_{eh}}{\pi}\right)^{1/3}$, where ϵ_o and ϵ_s are the dielectric constants in free space and in the semiconductor, respectively, and n_{eh} is the concentration of free electrons or holes. After carrier excitation, Δn_{eh} results in ΔE_g .

Bandgap reduction causes a red shift of the continuum absorption in semiconductors: $\Delta\alpha(n_{eh}, E) = \frac{C}{E}\sqrt{E - E_g - \Delta E_g(n_{eh})} - \frac{C}{E}\sqrt{E - E_g}$. It predicts that $\Delta\alpha$ is always positive. The nearer to the bandgap, the more rapid decreasing of $\Delta\alpha$. The change of refractive index is also calculated by applying the KK integrals. Due to bandgap renormalization, the largest change of refractive index is near the bandgap and it leads to a negative change of n at energies above the bandgap.

2-2.3 Free-Carrier Absorption

We have mentioned the changes of absorption coefficient and refractive index due to band filling and bandgap renormalization effects. Furthermore, in Drude model, a free carrier in the interband can absorb a photon and move to a higher energy state. The free carrier absorption is also called plasma effect. The change of refractive

index is $\Delta n = -\left(\frac{e^2 \lambda^2}{8\pi^2 c^2 \epsilon_0 n}\right)\left(\frac{N}{m_e} + \frac{P}{m_h}\right)$, where λ is the photon wavelength, m_e and m_h are the effective mass of electrons and holes, respectively. Free-carrier absorption causes a negative change of refractive index n .

We have introduced the concepts of carrier dynamics and the background of refractive index change. To find out the ultrafast behavior of InGaAs_{1-x}N_x SQW, the experimental setup of time-resolved photoreflectance will be demonstrated in the following chapter.



Chapter 3 Experiments

3-1 Principle of Femtosecond Time-Resolved Measurement

Ultrashort pulse laser has become a useful tool to investigate ultrafast carrier dynamics. The pulse-width of the laser can achieve femtoseconds (10^{-15} sec) and it is short enough to measure scattering/relaxation processes in materials.

When a short pulse is incident into the surface of a semiconductor, electrons will transit from valence band to conduction band then relax back to valence band through various relaxation regimes and processes, e.g., carrier-carrier or carrier-phonon scattering as described in Chapter 2. The process of relaxation changes dielectric constant (ϵ) in the material, and then affects its absorption/reflection rate. From the Fermi's golden rule, the change of reflection rate is proportional to the number of carriers. The carrier density is estimated using the simple relation: $\frac{\Delta R}{R} = \frac{4}{n^2 - 1} \Delta n$

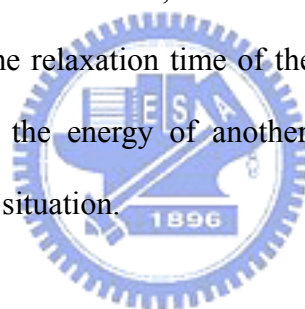
with the change of refractive index from the Drude model, where $\Delta n = -Ne^2 / 2nw^2 m^* \epsilon_0$, n is the refractive index of sample, N is carrier density, e is elementary charge, m^* is the effective mass of the conducting electrons, and ϵ_0 is the permittivity of free space. Through a weaker (probe) pulse laser detecting the reflection/transmission continuously, we can understand the phenomenon of carrier dynamics.

The most common technique is pump-probe reflection/transmission measurement. The spot size of the probe beam on the sample is smaller than that of the pump to ensure measuring a uniform photoexcited region. We control the optical path length of pump beam to reach the goal of temporal analysis.

Figure 3-1 shows the illustration of the principle of this technique. Assume that

the dotted line represents the temporal change of reflection/transmission rate of the sample after absorbing the pump pulses, and then the probe pulses incidence onto the sample in a delay time t to probe the signal of reflection/transmission. The third part of the figure is the voltage signal transferred from a detector modulated with a chopper. $I_0(t)$ is the DC value which represents the intensity of reflection rate R ; $\Delta I(t)$ is the AC value which represents the change of reflection ΔR . If dividing $\Delta I(t)$ by $I_0(t)$, we can get a dimensionless signal of $\Delta R/R$. Continuously controlling the time delay t , we will fully measure the temporal change of $\Delta R/R$.

In addition, if the relaxation time of carriers is longer than the time between two laser pulses, we will not be able to observe the complete relaxation. For example, the repetition rate of the laser is 75 MHz, there are 13.3 nanoseconds (ns) between two laser pulses. Suppose the relaxation time of the sample is longer than 13.3 ns, then the sample will absorb the energy of another pulse before it relaxes. The sample we used has no such a situation.



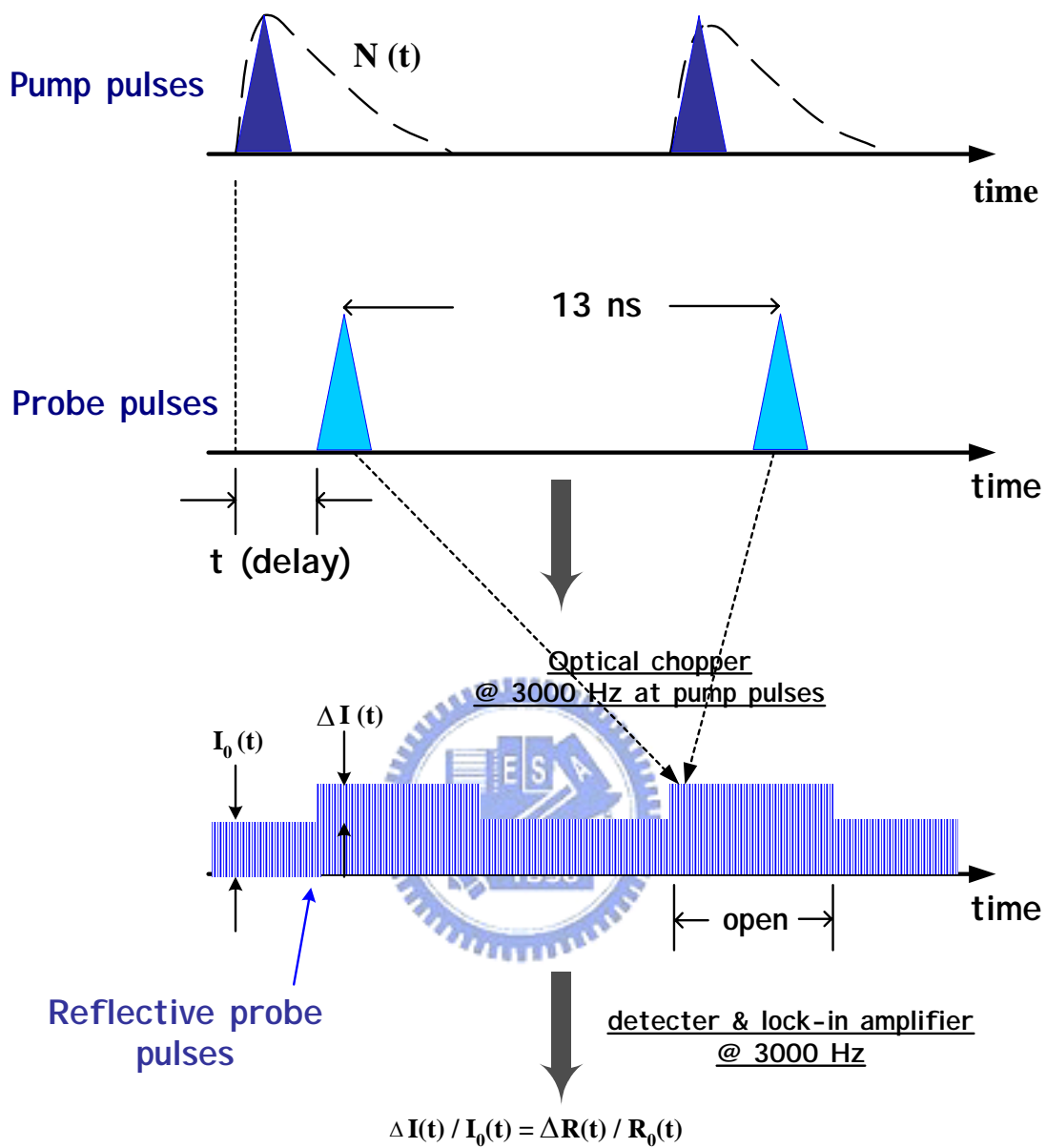


Fig. 3-1 The illustration for the principle of pump-probe technique.

3-2 Experimental System of Femtosecond

Time-Resolved Measurement

3-2.1 Ultrafast Laser System

A commercial Kerr-lens-mode-locked Ti:Sapphire laser (Coherent Mira900) is used as the light source which is pumped by a diode-pumped frequency-doubled Nd:YVO₄ laser (Coherent Verdi-8) with 527 nm with maximum power of about 8W. The structure of Ti:Sapphire laser is showed in Figure 3-2. The output wavelength is tunable from 700 nm to 900 nm using a prism sequence and a slit inside the laser cavity with a repetition rate of 75 MHz. Power of the output laser beam is less than 1W.

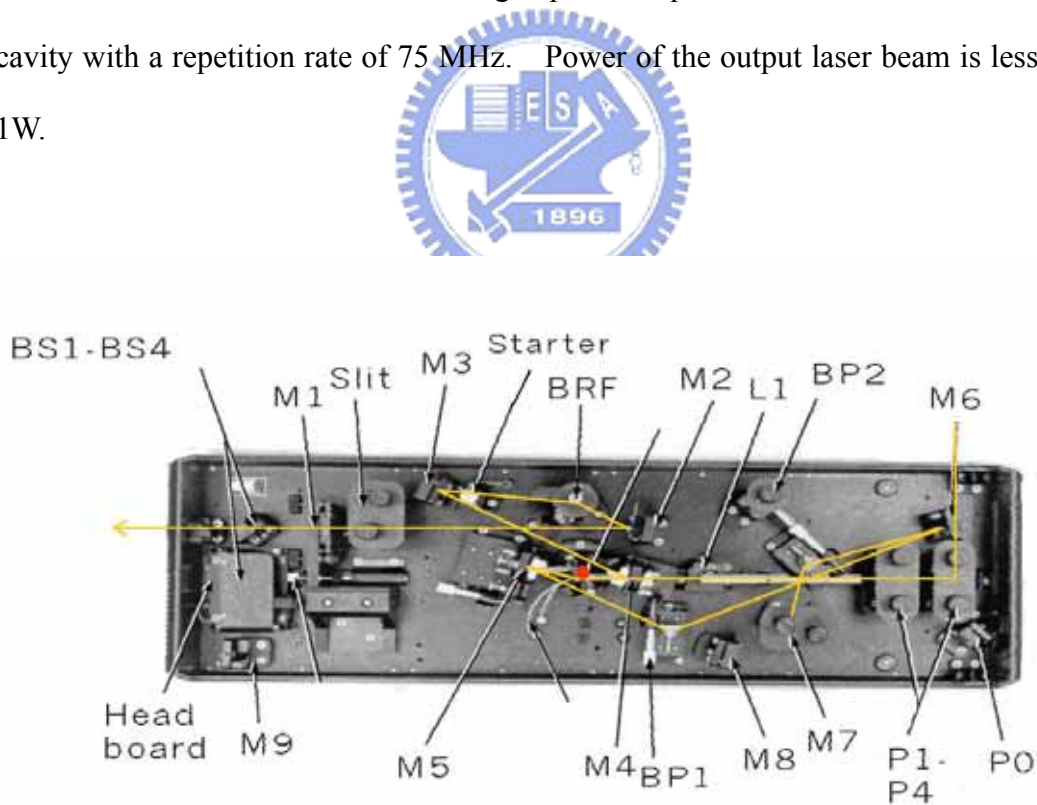


Fig. 3-2 The optical beam path within Coherent Mira-900.

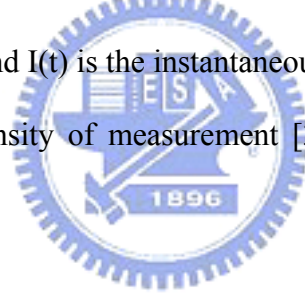
3-2.2 Autocorrelator

An autocorrelation system is for measuring the pulse-width of an ultrafast laser. A schematic of intensity autocorrelator is showed in Figure 3-3. A beamsplitter separates the laser beam into two beams, and one of them is temporally delayed by a translation stage. We put a beta barium borate (BBO) nonlinear optical crystal at the overlapped focal point of these two beams. The autocorrelation signal comes from second harmonic generation (SHG) of BBO is detected by a silicon detector. The detector receives the frequency-doubled intensity of two laser beams which is determined by autocorrelation function:

$$S(\tau) \propto \int I(t) \times I(t - \tau) dt,$$

where τ is the time delay, and $I(t)$ is the instantaneous intensity.

Figure 3-4 shows the intensity of measurement [31]. The pulse-width is 230fs obtained by Guassian fitting.



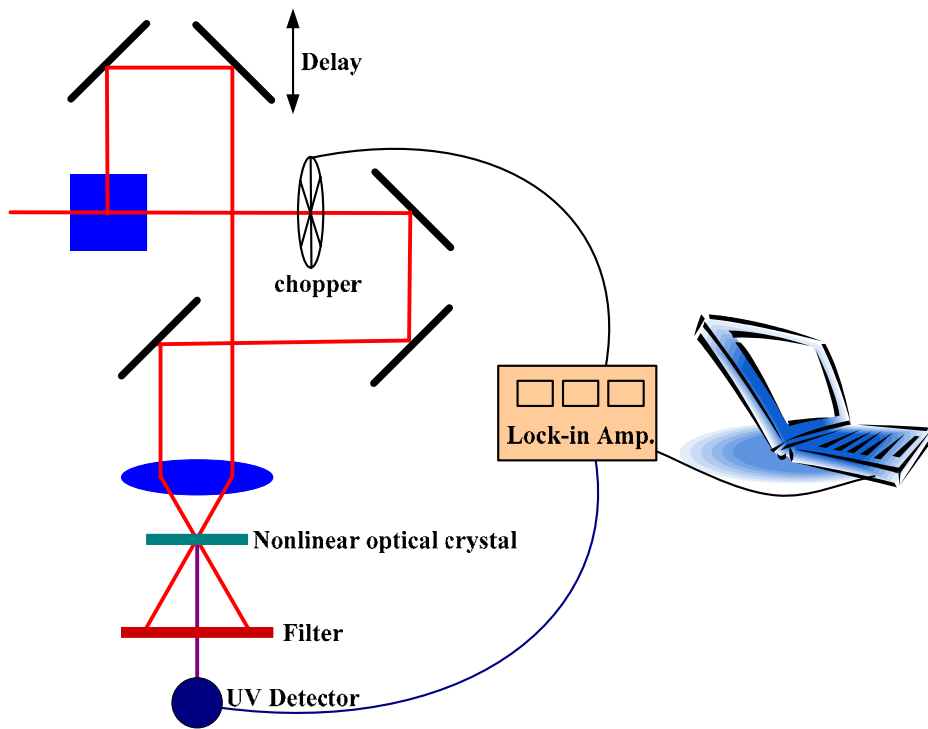


Fig. 3-3 Sketch diagram of the intensity autocorrelator.

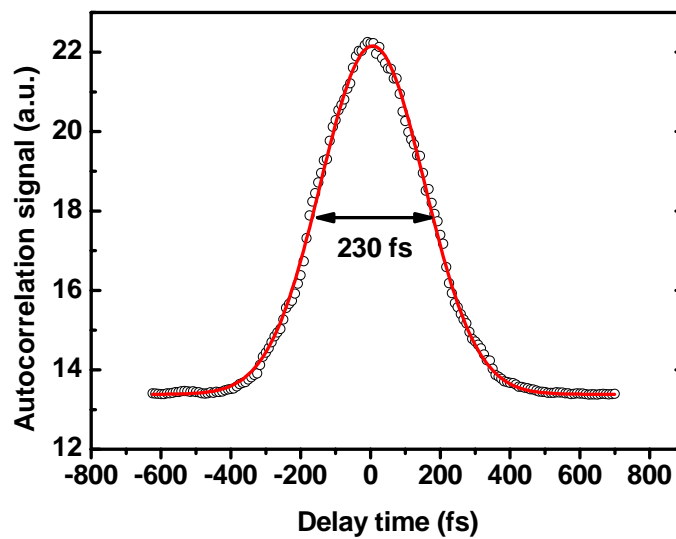


Fig. 3-4 The autocorrelation trace.

3-2.3 Experimental Setup of Pump-probe Measurement

The schematic diagram of pump-probe setup performed at room temperature is shown in Figure 3-5. The mode-locked Ti:Sapphire laser described in Section 3-2.1 is the light source. After a variable neutral density filter (ND1) which is for attenuating the power of the laser beam, a 50/50 beamsplitter (BS) splits the beam into pump and probe beams. Another variable neutral density filter (ND2) is used to attenuate the power of probe beam and keep the pump probe ratio 160:1.

A chopper with 25 KHz is used to control pump beam and modulate its frequency for Lock-in Amplifier receiving the signal. A time delay stage with 1.25 μm resolution is applied to change the optical path length of pump beam, resulting in a relative time delay between pump and probe pulses. A half-wave ($\lambda/2$) plate rotating the polarization of probe beam by 90° is for avoiding the optical coherent artifacts.

Pump and probe beams meet each other on the sample. Each of them focuses separately by two convex lenses with focal lengths of 10 and 5 cm. The spot size of focused pump beam is about 300 μm . A CCD camera is adopted to ensure the spatial overlap of pump and probe beams. A silicon photodiode detector (HAMAMATSU C5460) is for receiving the reflected light of probe beam and passing it to the lock-in amplifier (Stanford Research System, Model SR830). The final data as a function of temporal delay of pump and probe beams is then showed on a PC monitor.

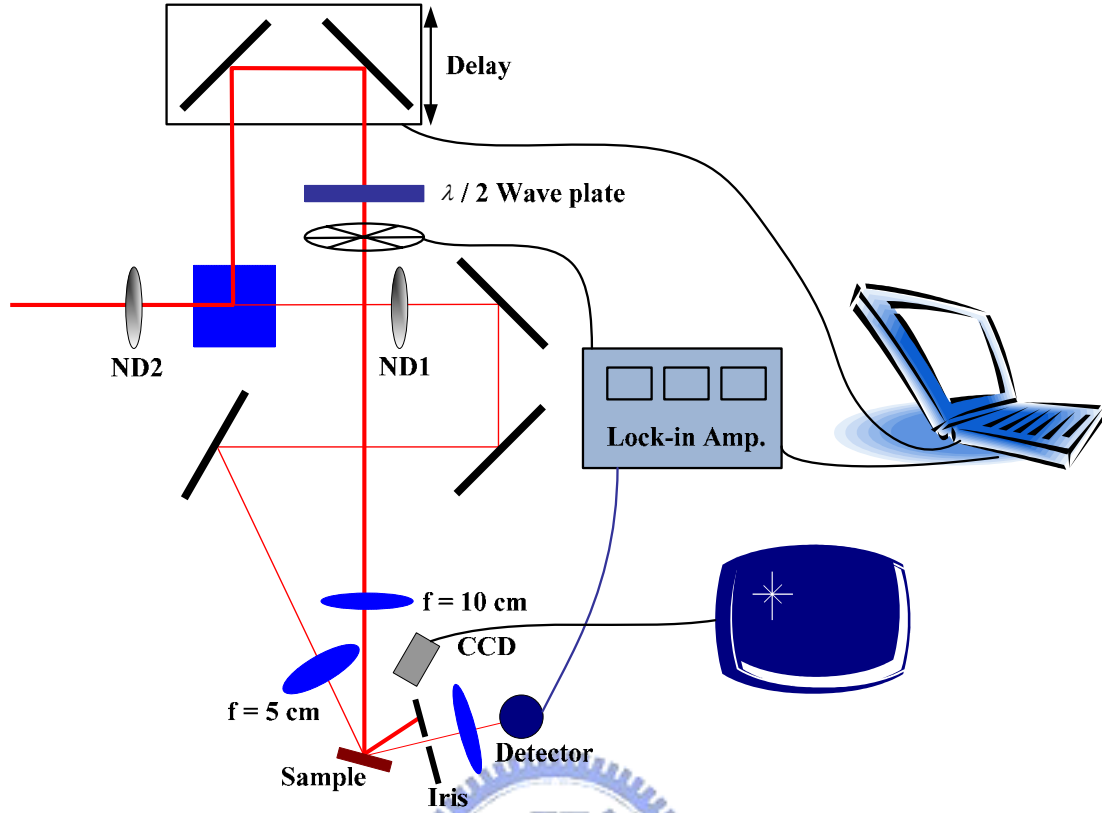


Fig. 3-5 Femtosecond time-resolved photorefractance measurement system.

3-3 Zero Delay Point of the System

To find the zero delay point of pump and probe beams is a very important step in this experiment. We focused the two beams respectively on a BBO crystal, and then observed frequency-doubled light after the overlapping point. The position of time delay stage where BBO has the strongest intensity is defined to be zero delay point.

Type- I phase matching condition of SHG is given by $\Delta k = k(\omega_2) - 2k(\omega_1) = 0$,

where $k(\omega_1) = \frac{2\pi n_1(\omega_1)}{\lambda_1}$, $k(\omega_2) = \frac{2\pi n_2(\omega_2)}{\lambda_2}$, $\lambda_1 = 2\lambda_2$, and

$n_2(\omega_2) = n_e(\omega_2, \theta) = \left(\frac{\cos^2 \theta}{n_o^2(\omega_2)} + \frac{\sin^2 \theta}{n_e^2(\omega_2)} \right)^{-1/2}$, respectively. Here θ is the phase

matching angle, ω_1 is the fundamental angular frequency, $\omega_2 = 2\omega_1$, n_o is the

ordinary refractive index, and n_e is the extra-ordinary refractive index.

3-4 InGaAsN Single Quantum Well Structures

The samples we used in our measurement are InGaAs(N)/GaAs single quantum wells which were grown by Tansu *et al.*. Several dilute-nitride $\text{In}_{0.4}\text{Ga}_{0.6}\text{As}$ single quantum wells on GaAs substrate were developed by low-pressure metal-organic chemical vapor deposition (LP-MOCVD) method during the past few years. Trimethylgallium, trimethylaluminium, and trimethylindium are used as group-III sources. AsH_3 and PH_3 are used as group-V precursor and U-dimethylhydrazine is N precursor. The doping sources are SiH_4 and diethylzinc for n and p dopants, respectively. The active layers are 60 Å $\text{In}_{0.4}\text{Ga}_{0.6}\text{As}_{1-x}\text{N}_x$ QW, sandwiched with various barrier materials: 3000 Å in GaAs confining layers, 75 Å in $\text{GaAs}_{0.85}\text{P}_{0.15}$ tensile barriers, and 30 Å in $\text{GaAs}_{0.67}\text{P}_{0.33}$ buffer layers. In and N contents of the InGaAsN material were determined from high-resolution x-ray diffraction and secondary mass ion spectroscopy. The N composition x in the structures are 0% and 2%, respectively. Figure 3-6 is the schematic diagram of the samples. The growing details of InGaAs(N) can be consulted in Refs. [26][27].

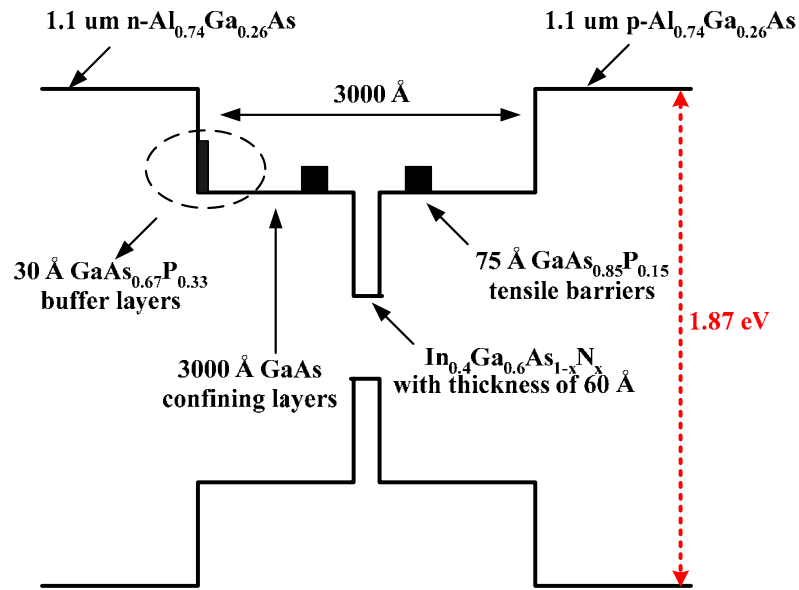


Fig. 3-6 Cross-sectional schematic conduction band diagram of the $\text{In}_{0.4}\text{Ga}_{0.6}\text{As}_{1-x}\text{N}_x$ SQW (Ref. [26]).

Figure 3-7 is the high resolution transmission electron microscopy (HRTEM) image of the interface quality of $\text{In}_{0.4}\text{Ga}_{0.6}\text{As}_{0.98}\text{N}_{0.02}$ SQW [28]. The rough interface seems to have dark island regions which is about 2-3 nm.

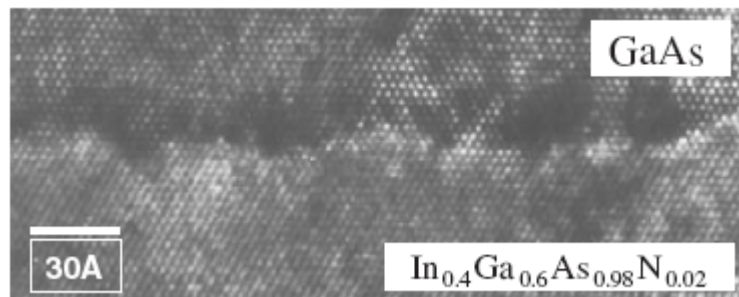


Fig. 3-7 HRTEM image of $\text{In}_{0.4}\text{Ga}_{0.6}\text{As}_{0.995}\text{N}_{0.005}/\text{GaAs}$ SQW.

3-5 Method and Steps of Pump-probe Measurement

After setting up the experimental system, the steps of the experiment are as follows:

- 1. Turn on the laser:** Turn the laser on and tune the wavelength to 820/880 nm

then adjust it to mode-locking. Use the spectrometer to observe the spectrum of laser beam and ensure the stability of it.

- 2. Stick the sample on:** Obstruct the laser beam before sticking on the sample to prevent reflected light will be incident back into the laser cavity. Then stick the sample on a three-dimensional stage.
- 3. Measure the spectrum at room temperature:** Ensure the overlapping of pump and probe beams hourly during the measurement. Control the polarization of pump and probe beams perpendicular to each other to avoid interference. Measure ΔR under different pumping powers.



Chapter 4 Results and Discussion

The pump pulses generate carriers through interband transition in semiconductors can be probed by the time-resolved photoreflectance. After pumping, the various carrier relaxation and decay mechanisms inside semiconductors cause the change of complex refractive index. This brings about the change in reflectivity of probe beam. So from detecting the intensity change of the reflected probe beam, we can get the status of carrier decaying. The reflectivity change can be modeled by the absorption change due to band filling (BF) effect, band gap renormalization (BGR), plasma screening effect, enhancement of absorption, and interband absorption of photons by free carriers (FCA).

The change of reflectivity (ΔR) is because of the change of complex refractive index ($n + i\kappa$). The major contribution to the change of $n + i\kappa$ is written as $\Delta n = \Delta n_{BF+BGR} + \Delta n_{FCA}$. ΔR is the difference between the reflectivity R with and without pumping, which is calculated as $\Delta R(h\nu) = R(n', \kappa'; h\nu) - R(n, \kappa; h\nu)$. The reflectivity R is given by $R(n, \kappa; h\nu) = \frac{[n(h\nu) - 1]^2 + \kappa^2(h\nu)}{[n(h\nu) + 1]^2 + \kappa^2(h\nu)}$, where κ is related to the absorption coefficient by $\kappa(h\nu) = \frac{\lambda}{4\pi} \alpha(h\nu)$, $\Delta\kappa(h\nu) = \frac{\lambda}{4\pi} \Delta\alpha(h\nu)$, and n' and κ' are the modified real and imaginary parts of refractive index with pumping (under the presence of the carrier density N), respectively.

We have measured $\text{InGaAs}_{1-x}\text{N}_x$ SQWs with $x = 0$ and 0.02 at 820 and 880 nm, separately. Since the band gap energy of the GaAs confining layer corresponds to the wavelength of 870 nm, tuning the pumping photon wavelength to 880 nm is enough to avoid absorption of the GaAs confining layer. The bandgap of $\text{In}_{0.4}\text{Ga}_{0.6}\text{As}$ and $\text{In}_{0.4}\text{Ga}_{0.6}\text{As}_{0.98}\text{N}_{0.02}$ SQW are $1.2 \mu\text{m}$ and $1.45 \mu\text{m}$, respectively. The absorption curve of GaAs is presented in Figure 4-1, the absorption coefficient

decreases immediately in photon wavelength from 870 to 1000 nm, and its value at 870 nm is far more than that at 880 nm [29]. We have reduced the absorption of GaAs effectively when tuning the pumping wavelength to 880 nm. The definition of penetration depth is the reciprocal of absorption coefficient. From Figure 4-1, we can extract the penetration depth of GaAs at 800 and 880 nm. They are 1.43 μm and 1000 μm , respectively. As we know, the thickness of confining layer GaAs is 0.3 μm , so the intensity of the laser beam which is incident into the quantum well remains $0.81I_0$ at 800 nm and $0.9997I_0$ at 880nm, where I_0 is the incident intensity of the beam. Therefore, the single quantum well can efficiently absorb the pumping laser beam. Notice that the exciton resonances are very weak in bulk GaAs and thus can only be observed at very low temperature [30].

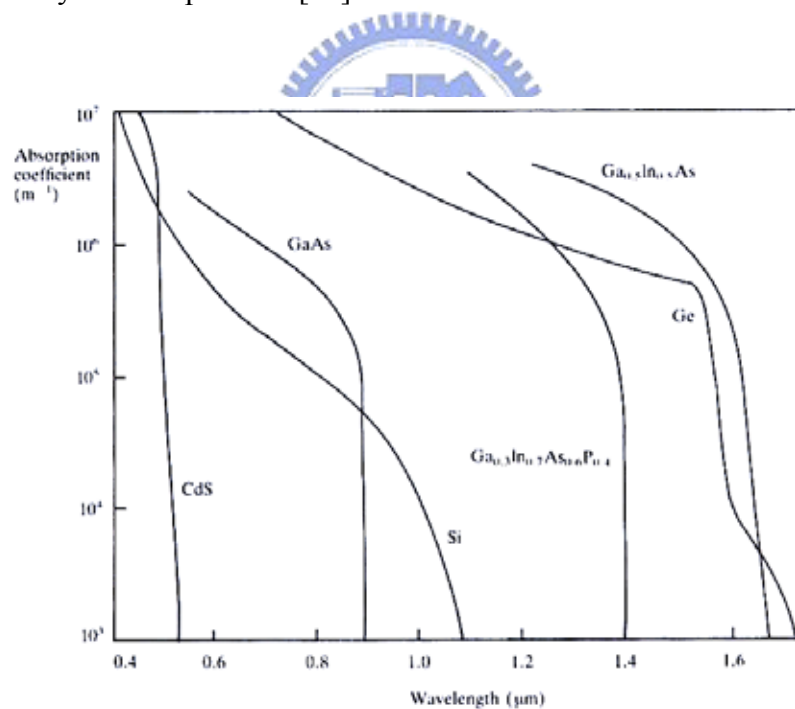


Fig. 4-1 Absorption curve of GaAs (Ref. [29]).

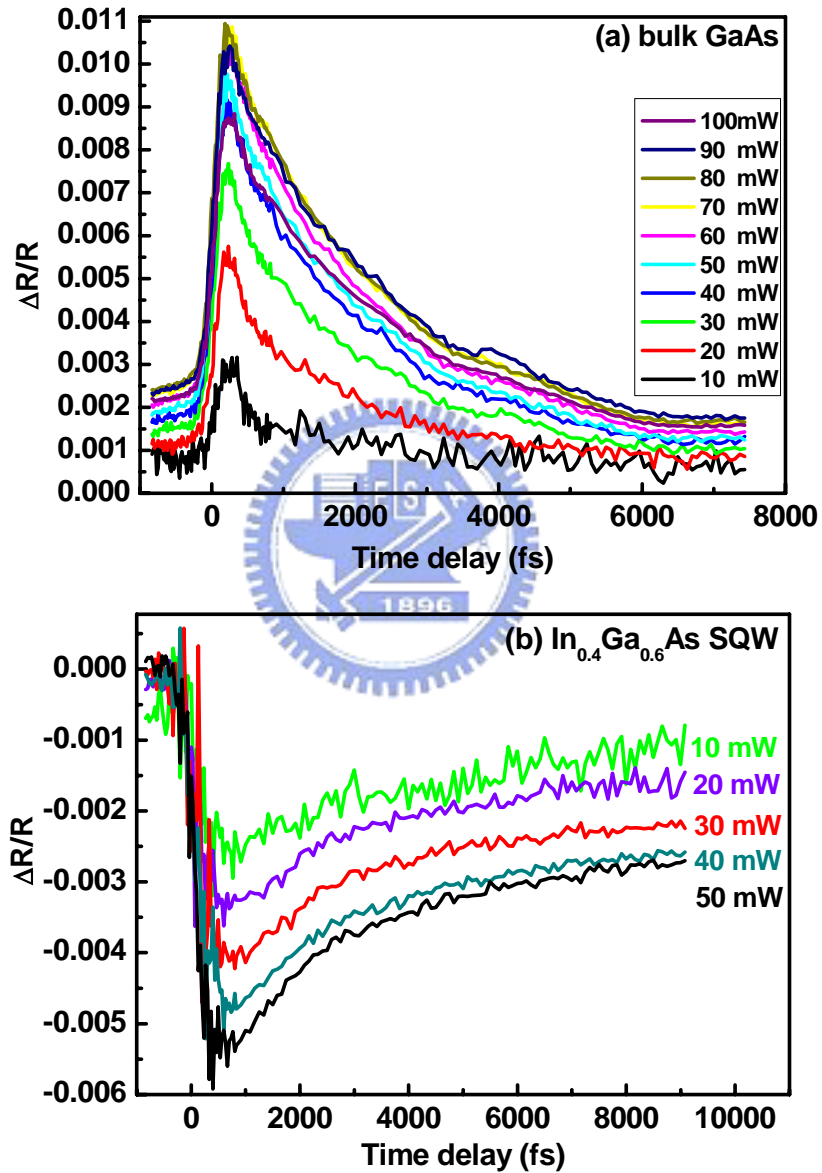
We extract the data from 10 to 50 mW and obstruct the laser beam between every measuring to reduce the thermal effect. Therefore, the thermal effect is not considered in our experiments.

4-1 Ultrafast Time-Resolved Photoreflectance of

$\text{In}_{0.4}\text{Ga}_{0.6}\text{As}_{1-x}\text{N}_x$ SQW

In order to describe a complete sketch of the optical properties of $\text{In}_{0.4}\text{Ga}_{0.6}\text{As}_{1-x}\text{N}_x$, we review some results of Y. H. Lin in 2005 [31]. Keeping the pumping wavelength at 800 or 820 nm, whose corresponding energies are both above the bandgap of GaAs, Figure 4-2 shows the results of time-resolved photoreflectance of bulk GaAs and $\text{In}_{0.4}\text{Ga}_{0.6}\text{As}_{1-x}\text{N}_x$ ($x = 0$ and 0.02) SQW with pumping power varying from 10 to 100 mW, respectively. The fast rising and decaying responses in Figure 4-2(a), (b), and (c) are because the generation of carriers occupies the optical-coupled transition states. After the absorption, the carriers scatter out of their initial states and subsequent relax toward the band edges through carrier-carrier and carrier-phonon scattering. In bulk GaAs, there is a positive $\Delta R/R$, however, $\text{In}_{0.4}\text{Ga}_{0.6}\text{As}_{1-x}\text{N}_x$ SQWs have the opposite behavior with GaAs with negative $\Delta R/R$. It is amazing to find that the thickness of these quantum wells is only 60 Å, we still can distinguish the huge differences of carrier dynamics between bulk GaAs and $\text{In}_{0.4}\text{Ga}_{0.6}\text{As}_{1-x}\text{N}_x$ SQWs. The positive ΔR so as positive index change is mainly due to band filling effect because the pumping photon energy is above the bandgap of bulk GaAs. On the other hand, the negative change of transient reflectance of $\text{In}_{0.4}\text{Ga}_{0.6}\text{As}_{1-x}\text{N}_x$ SQWs corresponds to a negative index change. The exact mechanism of negative index change is very complicated and still not fully understood. Because the thickness of these quantum wells is only 60 Å and the pumping photon energy is above the bandgap of the GaAs confining layer, we speculate that the carriers are mainly excited in the confining layer then quickly trapped into the quantum wells of both InGaAs and InGaAsN SQW samples. Due to

the much smaller bandgap, the band filling would not contribute to index change that results in negative change of transient reflectance from the band gap renormalization and the free-carrier absorption (FCA) or re-excitation of trapped carriers into the conduction band [32].



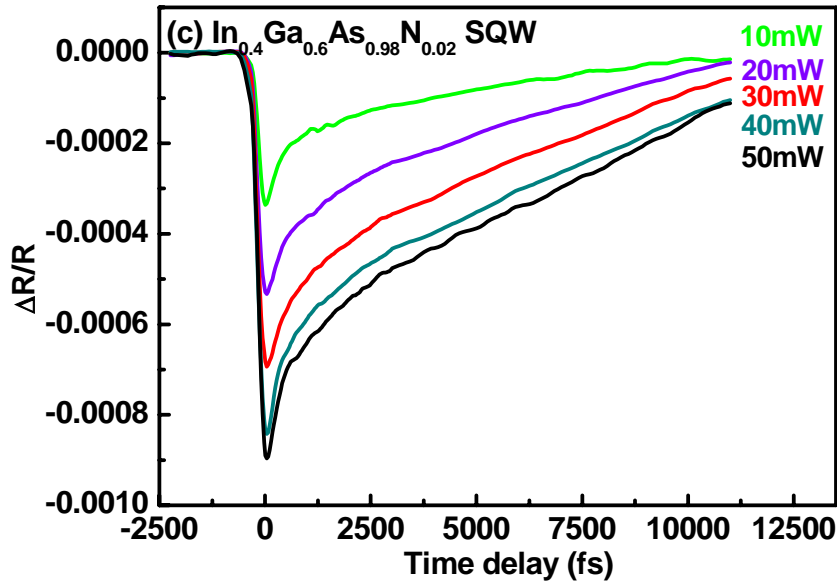


Fig. 4-2 The pump-intensity dependent time-resolved photoreflectance of (a) bulk GaAs, (b) $\text{In}_{0.4}\text{Ga}_{0.6}\text{As}$ SQW pumped at 800 nm from [31], and (c) $\text{In}_{0.4}\text{Ga}_{0.6}\text{As}_{0.98}\text{N}_{0.02}$ SQW pumped at 820 nm.

Although the mechanism of carrier relaxation in $\text{In}_{0.4}\text{Ga}_{0.6}\text{As}_{1-x}\text{N}_x$ SQWs is distinct from that in bulk GaAs, the GaAs confining layer whose bandgap is 870 nm makes the carrier relaxation complicated when pumping wavelength is at 800 or 820 nm. It can truly avoid the absorption of GaAs confining layer by adjusting the pumping wavelength to 880 nm. Shown in Figure 4-3 are the results of time-resolved photoreflectance of $\text{In}_{0.4}\text{Ga}_{0.6}\text{As}_{1-x}\text{N}_x$ ($x = 0$ and 0.02) SQWs with pumping power varying from 10 to 60 mW at 880 nm. It reveals a contrary result comparing to the previous measured results in Figure 4-2. The measured reflectance turned to be positive at 880 nm. The positive change of transient reflectance is due to the band filling effect, indicating a positive change of refractive index ($\Delta n > 0$) [24]. The opposite phenomenon may result from different initial occupied states of the photo-excited carriers for two pump wavelengths. With pumping wavelength < 820 nm, the carriers are generated in confining layer GaAs during pumping, and then the

quantum well capture those carriers in a short time. After carriers are trapped in $\text{In}_{0.4}\text{Ga}_{0.6}\text{As}_{1-x}\text{N}_x$ SQWs, there will be no band filling effect but the increase of carriers in the well could cause bandgap shrinkage and therefore leads to negative index change so as the negative ΔR .

Locations of the peaks in Figure 4-3(a) are a little different with various pumping power, the reason might be fluctuation of our laser or vibration of the step-motor. Besides, we have adjusted the polarization of pumped and probe beam perpendicular to each other, the interference caused by overlapping of pumped and probe beam occurs around the zero delay point which is clearly seen in Figure 4-3(b). We extract every peak at different pumping power and sketch them in Figure 4-4 to expose the tendency.



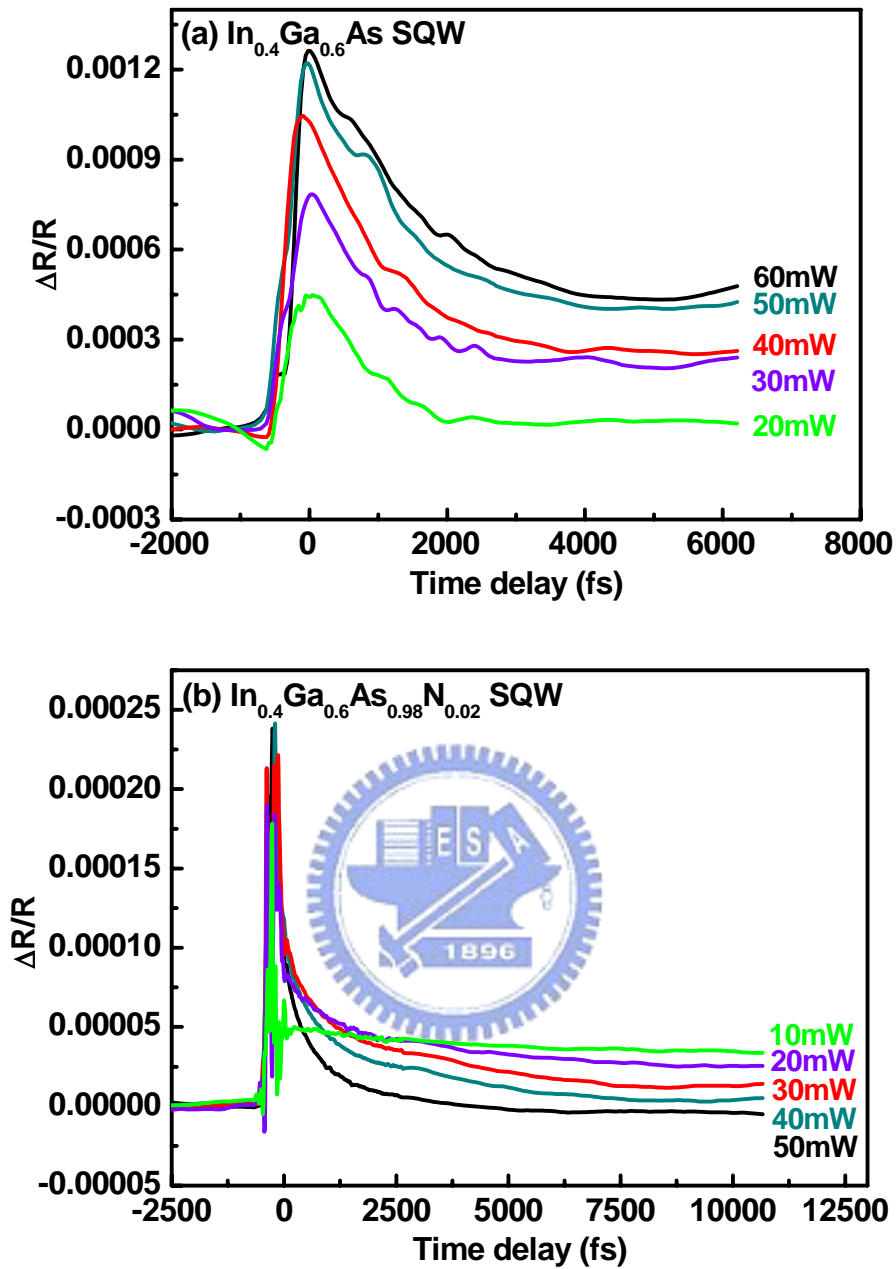


Fig. 4-3 The pump-intensity dependent time-resolved photoreflectance of (a) $\text{In}_{0.4}\text{Ga}_{0.6}\text{As}$ SQW and (b) $\text{In}_{0.4}\text{Ga}_{0.6}\text{As}_{0.98}\text{N}_{0.02}$ SQW pumped at 880 nm.

Due to the interference of pumped and probe beams nearby the zero time delay, it is hard to find the exact location of peaks with pumping wavelength at 880 nm in Figure 4-3(d). By fitting the curves with a Lorentzian and a biexponential function to all of the photoreflectance curves, the measured peak amplitude of ΔR versus pumping

power density of $\text{In}_{0.4}\text{Ga}_{0.6}\text{As}$ SQW is displayed in Figure 4-4. The magnitude of ΔR peak is proportional to the density of carriers accumulated in the allowed optical transition states after photoexcitation. The carrier density N can be calculated using the relation mentioned in Section 3-1 based on the Drude model: $\frac{\Delta R}{R} = \frac{4}{n^2 - 1} \Delta n$, where $\Delta n = -Ne^2 / 2n\omega^2 m^* \epsilon_0$. The estimated carrier densities are listed in Table 4-1.

Due to absorption by the GaAs confining layer, the carrier densities with pumping wavelength < 820 nm are an order of magnitude larger than those of pumped at 880 nm for both samples but the larger carrier density for InGaAs SQW than for InGaAsN SQW. It is worth to note that when pumped at 880 nm, whose photon energy is below GaAs bandgap but above those of both samples, the carrier densities are nearly the same at the lowest pumping; whereas, with increasing pumping power density, the carrier density increases faster than that of InGaAsN SQW.

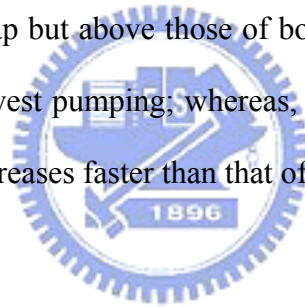
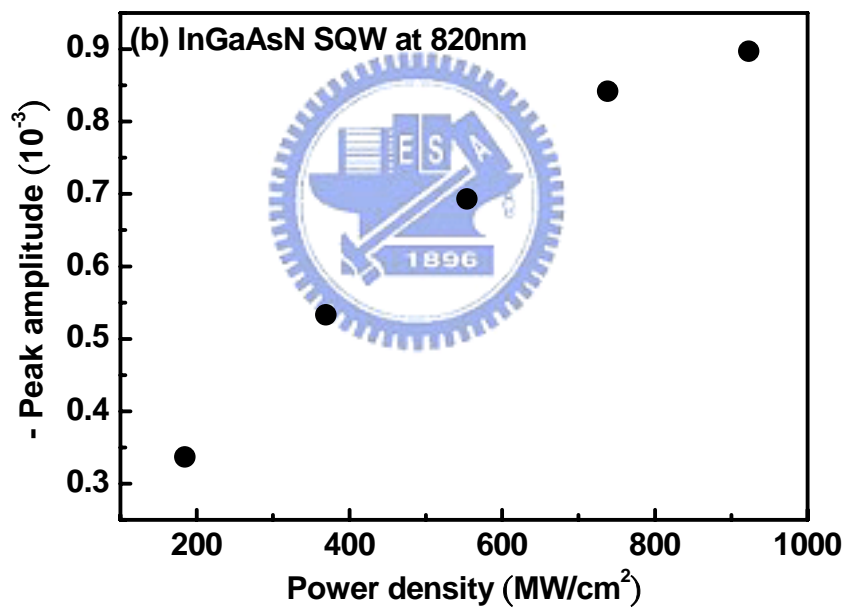
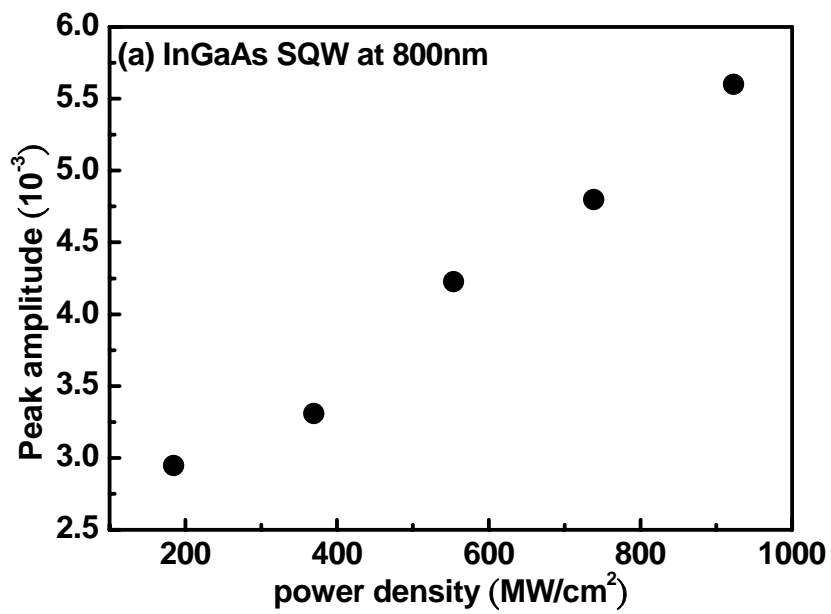


Table 4-1. List of carrier densities of $\text{In}_{0.4}\text{Ga}_{0.6}\text{As}$, $\text{In}_{0.4}\text{Ga}_{0.6}\text{As}_{0.98}\text{N}_{0.02}$ with various pumping power.

Power density (MW/cm ²)	$\text{In}_{0.4}\text{Ga}_{0.6}\text{As}$		$\text{In}_{0.4}\text{Ga}_{0.6}\text{As}_{0.98}\text{N}_{0.02}$	
	N (10 ¹⁸ cm ⁻³)		N (10 ¹⁸ cm ⁻³)	
	800 nm	880 nm	820 nm	880 nm
184.6	6.19	0.11	0.83	0.12
369.2	6.95	0.78	1.31	0.30
553.8	8.87	1.36	1.70	0.39
738.4	10.07	1.82	2.07	0.46
923	11.76	2.12	2.21	0.51
1107.6	--	2.19	--	--

After being pumped to the higher states, carriers can diffuse in the 3000Å GaAs confining layer or be trapped into the quantum well. The band filling effect will not be obvious, so all of the carrier densities basically linearly increase with the pumping power for those pumping at wavelength < 820 nm in Figures 4-4(a) and (b). On the other hand, when pumping at 880 nm, carriers will localize in $\text{InGaAs}_{1-x}\text{N}_x$ single quantum well. The band filling effect dominates positive Δn and it will saturate at high pumping, that is because $\Delta\alpha$ is nonlinear, the relation of power density versus peak amplitude in Figure 4-4(c) and (d) is also nonlinear.



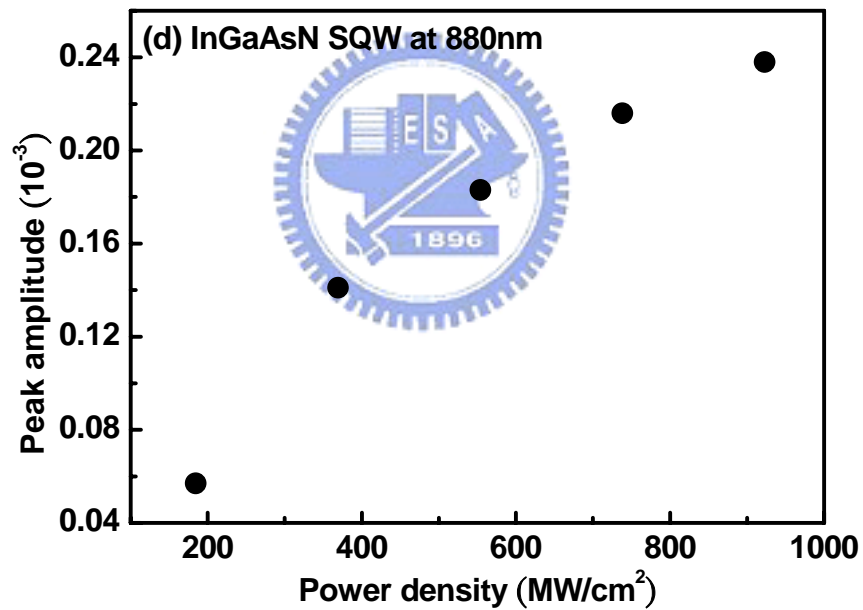
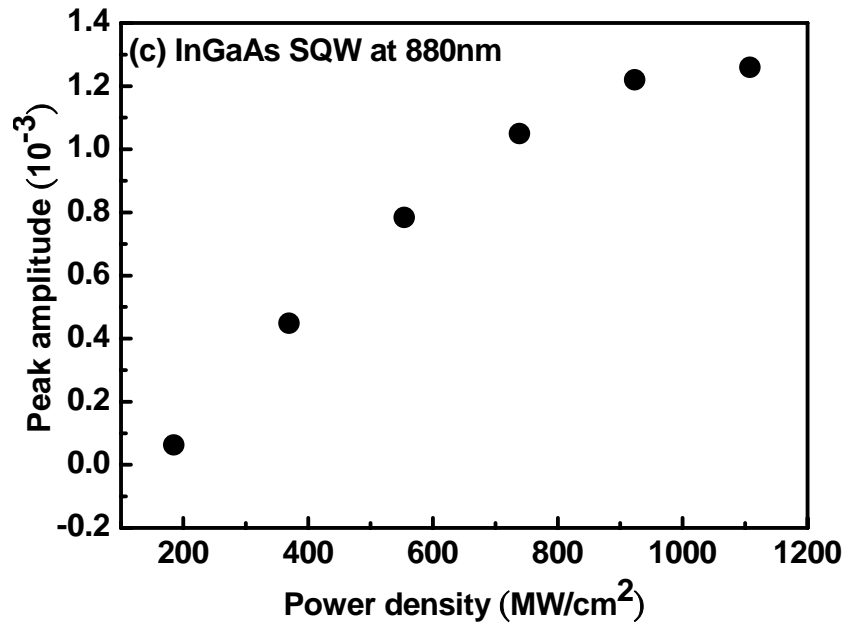


Fig. 4-4 The measured ΔR peak amplitude versus pumping power with pumping wavelength at 800/820 nm in (a) $\text{In}_{0.4}\text{Ga}_{0.6}\text{As}$ (b) $\text{In}_{0.4}\text{Ga}_{0.6}\text{As}_{0.98}\text{N}_{0.02}$ SQW and at 880 nm in (c) $\text{In}_{0.4}\text{Ga}_{0.6}\text{As}$ (d) $\text{In}_{0.4}\text{Ga}_{0.6}\text{As}_{0.98}\text{N}_{0.02}$ SQW.

4-2 Carrier Relaxation Time of InGaAs_{1-x}N_x SQW

We extract the relaxation time of carriers by fitting the experimental ΔR traces by using a double exponential decay function, $A \exp(-t/\tau_1) + B \exp(-t/\tau_2)$. We obtain the carrier decay time which is exhibited in Figure 4-5. The profile shows an initial fast decay followed by a slower relaxation [33]. The fast component of carrier lifetime approximates 2-3 ps with pumping wavelength at 800 nm and 1-2.5 ps at 880 nm. It does not change much with increasing pumping power. It is attributed to the carrier-carrier scattering. Because the pumping energy remains still, the rate of carrier-carrier scattering will basically not change even if the pumping power is already different. The later component of relaxation time is about several tens ps with pumping wavelength at 800 nm and 2-8 ps at 880 nm. As we know, τ_2 increases with increasing pumping power. The reason of these results is the appearance of hot phonons [24]. After receiving the energy from pumping beam, the carriers transfer their additional kinetic energy to phonons. Those phonons become hot phonons, and then transfer the energy back to carriers. Carriers which have more kinetic energy also take more time to relax to thermalization. As a result, it takes longer to decay when pumping power is rising. On the other hand, we could not judge the trend in Figure 4-5(a) due to the lack of statistics.

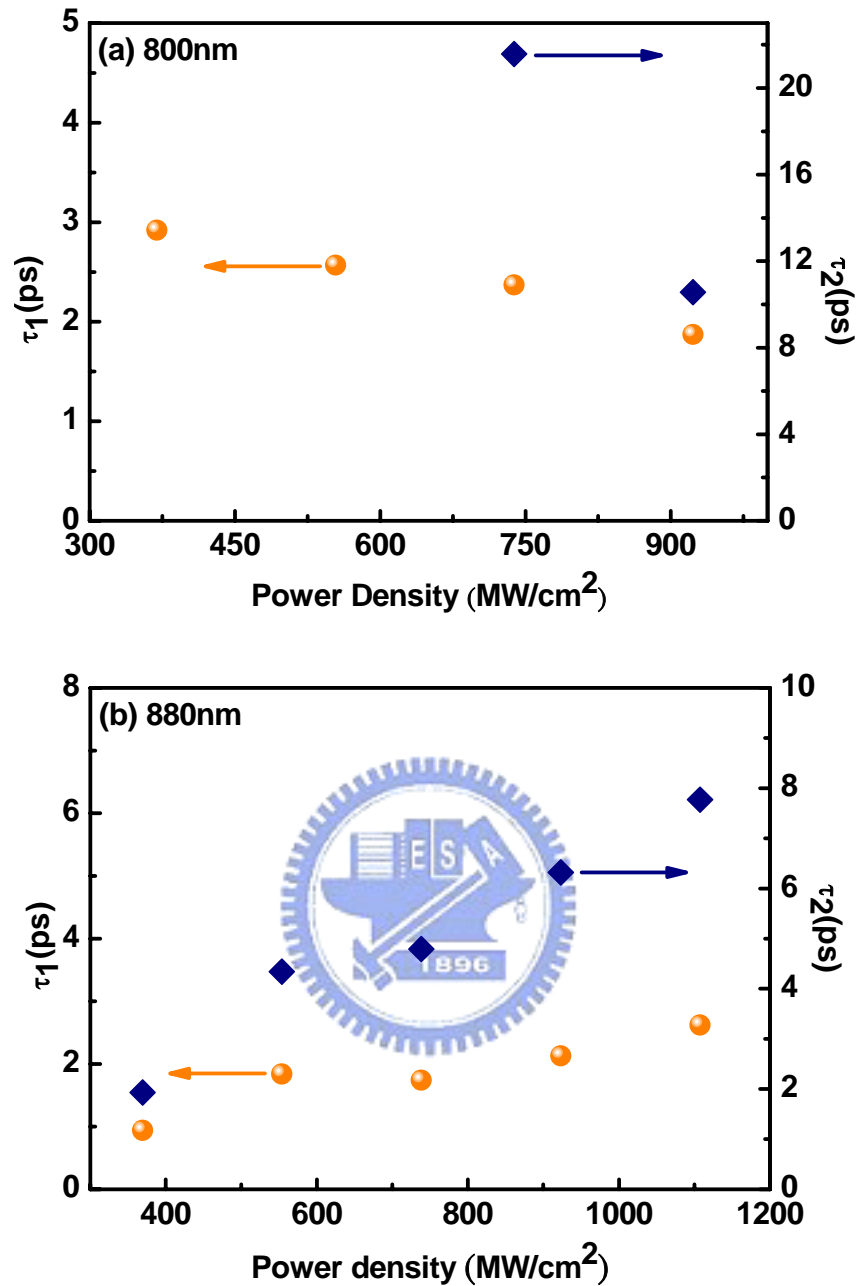
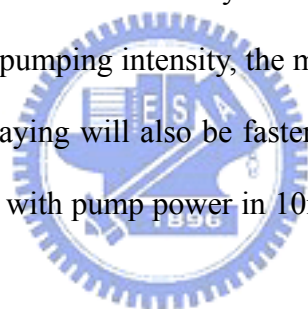


Fig. 4-5 The carrier lifetime versus pumping power in In_{0.4}Ga_{0.6}As SQW with pump wavelength at (a) 800 (b) 880 nm.

Figure 4-6 presents the carrier relaxation time fitted from Figure 4-3, and the illustrations represent In_{0.4}Ga_{0.6}As_{0.98}N_{0.02} SQW with the pumping wavelength at 820 and 880nm, respectively. In In_{0.4}Ga_{0.6}As_{0.98}N_{0.02} SQW, the photo-excited carrier could quickly and efficiently be trapped by the local defects (alloy fluctuation) due to

N-incorporation during or after they experienced electron-hole scattering to lose their excess kinetic energy. In Figure 4-6(a), the observed short relaxation time of ~1-2 ps is attributed to the carrier-carrier scattering; τ_1 is almost constant for various power densities. The longer decay time of 5-8 ps increases with the pumping power that is attributed to hot phonon decay. The mechanism of hot phonon has already reported in Section 4-1. After adjusting the pumping wavelength to 880 nm, we discover that the behavior of τ_2 is contrary to the second decay time at 820nm. Originally it takes 0.3-0.8 ps to relax in Figure 4-6(b), carrier-carrier scattering occurs at this moment. Then it takes 2-4.5 ps to accomplish the later relaxation process, which decreases when the pumping power increases. As we know, the sample has lasing characteristics [34], stimulated emission decay times faster than 10 ps have been noticed. The stronger of the pumping intensity, the more carriers will be in the upper state, and then the carrier decaying will also be faster [35]. Moreover, we can only see an exponential decay time with pump power in 10mW through large fluctuation at low pumping.



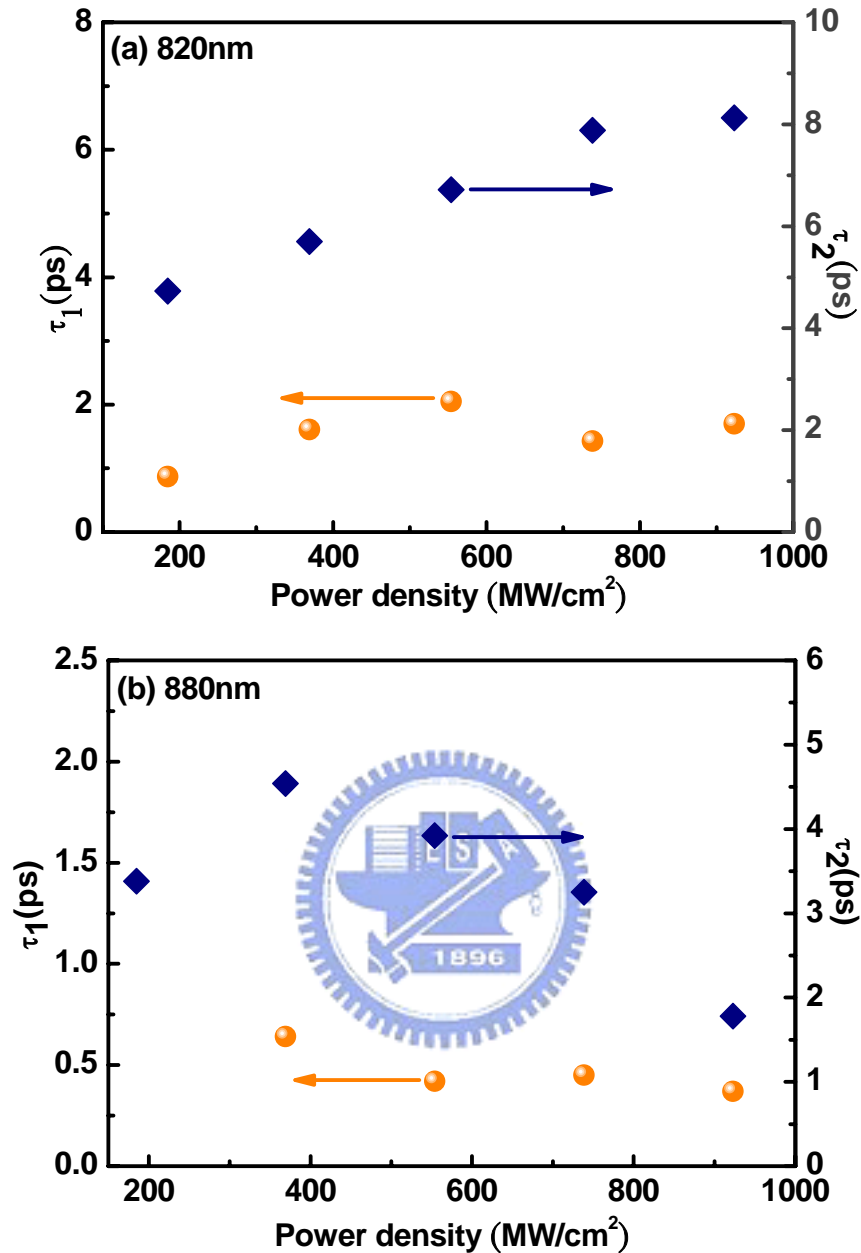


Fig. 4-6 The carrier lifetime versus pumping power in $\text{In}_{0.4}\text{Ga}_{0.6}\text{As}_{0.98}\text{N}_{0.02}$ SQW with pump wavelength at (a) 820 (b) 880 nm.

Comparing $\text{In}_{0.4}\text{Ga}_{0.6}\text{As}$ SQW with $\text{In}_{0.4}\text{Ga}_{0.6}\text{As}_{0.98}\text{N}_{0.02}$ SQW, it clearly reveals that $\text{In}_{0.4}\text{Ga}_{0.6}\text{As}$ SQW shows not only an order of magnitude $\Delta R/R$ larger than that of $\text{In}_{0.4}\text{Ga}_{0.6}\text{As}_{0.98}\text{N}_{0.02}$ SQW, but also a longer relaxation time. It is consistent with the time-resolved PL measurements which were done by Lifang *et al.* [19] and the below threshold modulation frequency response measurements which were studied by

Anton *et al.* [36]. This phenomenon can be explained by presence of defects after nitrogen incorporation. Some trap states are formed within the bandgap by defects, and they will capture excited carriers efficiently. The trap states act like nonradiative recombination centers. This process lasts a shorter time than the intraband relaxation, and that is why carrier lifetime in $\text{In}_{0.4}\text{Ga}_{0.6}\text{As}_{0.98}\text{N}_{0.02}$ is shorter. Besides, carriers in excited states above the conduction band minimum can also be trapped due to the localization of these trap states. Furthermore, the carrier density of $\text{In}_{0.4}\text{Ga}_{0.6}\text{As}_{0.98}\text{N}_{0.02}$ SQW is an order of magnitude smaller than that of $\text{In}_{0.4}\text{Ga}_{0.6}\text{As}$ SQW, which is mainly due to the bandgap of $\text{In}_{0.4}\text{Ga}_{0.6}\text{As}_{0.98}\text{N}_{0.02}$ being farther from the excited photon energy of 1.55eV.



Chapter 5 Conclusion and Perspectives

We have successfully studied the ultrafast time-resolved photoreflectance of $\text{InGaAs}_x\text{N}_{1-x}$ ($x = 0$ and $x = 2\%$) single quantum wells even with extremely thin thickness of 60 \AA and 3000 \AA wide GaAs confining layer. After tuning the pumping wavelength to 880nm , it effectively avoids the absorption of confining layer GaAs. It is interesting to find that the change of refractive index turns to be positive, which is because the band filling effect replaces the renormalization of bandgap.

The calculated carrier densities and estimated relaxation times of carriers are also demonstrated. As mentioned above, the bandgap will be reduced and the carrier dynamics will be very different after nitrogen incorporation. With pumping wavelength at 880nm , the shorter carrier lifetimes of $\text{In}_{0.4}\text{Ga}_{0.6}\text{As}$ and $\text{In}_{0.4}\text{Ga}_{0.6}\text{As}_{0.98}\text{N}_{0.02}$ SQW are both independent of pumping power, which indicates the mechanism of carrier-carrier scattering. Nevertheless, the longer lifetime is proportional to the pumping power in $\text{In}_{0.4}\text{Ga}_{0.6}\text{As}$ SQW and inversely proportional to the pumping power in $\text{In}_{0.4}\text{Ga}_{0.6}\text{As}_{0.98}\text{N}_{0.02}$ SQW. The explanation of this phenomenon is hot phonon decay for the former and stimulated emission for the later. In addition, carrier lifetime in $\text{In}_{0.4}\text{Ga}_{0.6}\text{As}_{0.98}\text{N}_{0.02}$ SQW is shorter than that in $\text{In}_{0.4}\text{Ga}_{0.6}\text{As}$ SQW, which is on account of the appearance of the local defect states during nitrogen doping.

There are still some ways to progress the experimental setup. Replacing the optical chopper by an AOM modulator can improve the signal to noise ratio; using a pair of prisms can compress the pulse width of laser. We will further measure the photoluminescence emission of $\text{In}_{0.4}\text{Ga}_{0.6}\text{As}_{0.98}\text{N}_{0.02}$ under various pumping power to ensure the behavior of diode laser. Moreover, different material of samples like ZnO thin films can be surveyed in the future.

References

- [1] A.Y. Polyakov, N.B. Smirnov, A.V. Govorkov, A.E. Botchkarev, N.N. Nelson, M.M.E. Fahmi, J.A. Griffin, A. Khan, S. Noor Mohammad, D.K. Johnstone, V.T. Bublik, K.D. Chsherbachev, M.I. Voronova, and V.S. Kasatochkin, *Solid-State Electron.*, **46**, 2147(2002)
- [2] H. P. Xin, and C. W. Tu, *Appl. Phys. Lett.*, **72**, 2442 (1998).
- [3] G. L. Belenky, C. L. Reynolds, D. V. Donetsky, G. E. Shtengel, M. S. Hybertsen, M. A. Alam, G. A. Baraff, R. K. Smith, R. F. Kazarinov, J. Winn, and L. E. Smith, *IEEE J. Quantum Electron.*, **35**, 1515 (1999).
- [4] N. Tansu, N. J. Kirsch, and L. J. Mawst, *Appl. Phys. Lett.* **81**, 2523 (2002).
- [5] N. Tansu, J. Y. Yeh, and L. J. Maest, *Appl. Phys. Lett.* **82**, 3008 (2003).
- [6] N. Tansu, J. Y. Yeh, and L. J. Maest, *Appl. Phys. Lett.* **82**, 4038 (2003).
- [7] N. T. Hashimoto, Kazuhiko Misawa, and Roy Lang, *Appl. Phys. Lett.* **82**, 2749 (2003)
- [8] G. Sucha, S. R. Bolton, D. S. Chemla, D. L. Sivco, and A. Y. Cho, *Appl. Phys. Lett.*, **65**, 1486 (1994).
- [9] P. Borri, W. Langbein, J. M. Hvam, and F. Martelli, *Phys. Rev. B.*, **59**, 2215 (1999).
- [10] P. Bhattacharya, S. Ghosh, S. Pradhan, J. Singh, W. zong-Kwei, J. Urayma, K. Kim, and T. B. Norris, *IEEE J. Quantum Electronics.*, **39**, 952 (2003).
- [11] D.E. Mars, D.I. Babic, Y. Kaneko, and Ying-Lan Chang, *J. Vac. Sci. Technol. B*, **17**, 1272 (1999)
- [12] A. Vinattieri, D. Alderighi, M. Zamfirescu, M. Colocci, A. Polimeni, M. Capizzi, D. Gollub, M. Fischer, and A. Forchel, *Phys. Stat. Sol. (a)*, **195**, 558 (2003)
- [13] LiFang Xu, D. Patel, and C.S. Menoni, *Appl. Phys. Lett.*, **89**, 171112 (2006)

- [14] Lifang Xu, D. Patel, G. Vaschenko, O. Anton, C. S. Menoni, J. Y. Yeh, T. T. V. Roy, L. J. Mawst, N. Tansu, CLEO/QELS '05, Baltimore, Maryland, USA.
- [15] R. A. Mair, J. Y. Lin, H. X. Jiang, E. D. Jones, A. A. Allerman, and S. R. Kurtz, *Appl. Phys. Lett.* **76**, 188 (2000).
- [16] A. Kaschner, T. Lüttgert, H. Born, A. Hoffmann, A. Yu. Egorov and H. Riechert, *Appl. Phys. Lett.* **78**, 1391 (2001).
- [17] A. Vinattieri, D. Alderighi, M. Zamfirescu, M. Colocci, A. Polimeni, M. Capizzi, D. Gollub, M. Fischer, and A. Forchel, *Appl. Phys. Lett.* **82**, 2805 (2003).
- [18] O. Anton, C. S. Menoni, J. Y. Yeh, L. J. Mawst, J. M. Pikal, and N. Tansu, *IEEE Photon. Technol. Lett.*, **17**, 953 (2005).
- [19] Lifang Xu, D. Patel, G. Vaschenko, O. Anton, C. S. Menoni, J. Y. Yeh, T. T. V. Roy, L. J. Mawst, N. Tansu, CLEO/QELS '05, Baltimore, Maryland, USA.
- [20] Andreas Othonos, *J. Appl. Phys.*, **83**, 1789 (1998).
- [21] D. H. Auston, S. McAfee, C. V. Shank, E. P. Ippen, and O. Teschke, *Solid-State Electron.*, **21**, 147 (1978).
- [22] W. Z. Lin, R. W. Schoenlein, E. P. Ippen and R. A. Logan, *Appl. Phys. Lett.*, **50**, 124 (1987).
- [23] R. L. Fork, B. I. Greene, and C. V. Shank, *Appl. Phys. Lett.*, **38**, 671 (1981).
- [24] J. Shah, *Ultrafast Spectroscopy of Semiconductors and Semiconductor Nanostructures*, Springer-Verlag, Berlin, (1996).
- [25] Nasser Peyghambarian, Stephan W. Koch, Andre Mysyrowicz, *Introduction to Semiconductor Optics*, (1993)
- [26] N. Tansu, N. J. Kirsch, and L. J. Mawst, *Appl. Phys. Lett.*, **81**, 2523 (2002).
- [27] N. Tansu, J. Y. Yeh, and L. J. Maest, *Appl. Phys. Lett.*, **82**, 3008 (2003).
- [28] H. C. Kuo, F. I. Lai, Y. H. Chang, M. Y. Tsai, S. Y. Kuo, S. C. Wang, N. Tansu, J. Y. Yeh, and L. J. Maest, *J. Appl. Phys.*, **44**, 6204(2005)
- [29] John Wilson, John Hawkes, *Optoelectronics: an introduction*, (1998)

- [30] D.S. Chuu and Ying-Chih Lou, *Phys. Rev. B*, **43**, 14 504 (1991)
- [31] Ying-Hsiu Lin, *The Ultrafast Time Resolved Photoreflectance Measurement of InGaAs_xN_{1-x} Single Quantum Wells*, National Chiao Tung University, (2005)
- [32] B. R. Bennett, R. A. Soref, and J. A. D. Alamo, *IEEE J. Quantum Electronics.*, **26**, 113 (1990).
- [33] Clementine Symonds, Juliette Mangeney, Guillaume Saint-Girons, and Isabelle Sagnes, *Appl. Phys. Lett.*, **87**, 012107 (2005)
- [34] N. Tansu, J. Y. Yeh, and L. J. Mawst, *IEEE J. Quantum Electron.*, **9**, 1220 (2003)
- [35] Umit Ozgur and Henry O. Everitt, *Phys. Rev. B*, **67**, 155308 (2003)
- [36] O. Anton, C. S. Menoni, J. Y. Yeh, L. J. Mawst, J. M. Pikal, and N. Tansu, *IEEE Photon. Technol. Lett.*, **17**, 953 (2005).

